SIAM J. SCI. STAT. COMPUT.
Vol. 4, No. 1, March 1983

0196-5204/83/0401-0001 $01.25/0

NUMERICAL EXPERIMENTS ON SOLVING THEODORSEN'S INTEGRAL EQUATION FOR CONFORMAL MAPS WITH THE FAST FOURIER TRANSFORM AND VARIOUS NONLINEAR ITERATIVE METHODS*

MARTIN H. GUTKNECHT†

Abstract. In [M. H. Gutknecht, Numer. Math., 36 (1981), pp. 405–429] we investigated several iterative methods for solving discretized versions of Theodorsen's nonlinear integral equation. Here we present corresponding numerical experiments and discuss some related questions, such as the application of a continuation method, the evaluation of the approximate mapping function, the selection of the appropriate type of approximation, and the use of preliminary maps to eliminate corners. Both the nonlinear SOR method and a related second order Euler method are seen to be very effective, even if the assumptions of the theory do not hold.

1. Introduction. Theodorsen's integral equation [4, p. 65] is a well-known basis for the numerical computation of the conformal mapping g of the unit disk D onto a starlike region Δ given by the polar coordinates τ, $\rho(\tau)$ of its boundary Γ. The mapping g is normalized by $g(0)=0$, $g'(0)>0$. It is uniquely determined by the boundary correspondence function θ, which is defined implicitly by

$$g(e^{it}) = \rho(\theta(t))\, e^{i\theta(t)} \quad (\forall t \in \mathbb{R}), \qquad \int_0^{2\pi} \theta(t)\, dt = 2\pi^2. \tag{1.0}$$

Theodorsen's integral equation simply states that $Y: t \mapsto \theta(t) - t$ is the conjugate periodic function of $X: t \mapsto \log \rho(\theta(t))$. A bibliography up to 1964 is contained in Gaier [4]; more recent work including [10], [15], [16], [21], [22] is referenced in [12].

Upon discretization—briefly described below—Theodorsen's integral equation becomes a fixed point equation

$$\mathbf{y} = \boldsymbol{\Phi}(\mathbf{y}) := \mathbf{K}_\Sigma \log \rho(\mathbf{t}+\mathbf{y}) \tag{1.1}$$

for $\mathbf{y} \in \mathbb{R}^{2N}$. Here $\mathbf{t} := (k\pi/N)_{k=0}^{2N-1}$ is constant, $\mathbf{x} := \log \rho(\mathbf{t}+\mathbf{y})$ is the vector obtained by componentwise evaluation, $\mathbf{y}$ approximates $Y(\mathbf{t})$, and $\mathbf{K}_\Sigma$ is a circulant skew-symmetric Toeplitz matrix. The product $\mathbf{K}_\Sigma \mathbf{x}$ can be calculated in $O(N \log N)$ arithmetic operations by using the fast Fourier transform (FFT) [11], [15].

If the discretization is based on trigonometric interpolation, $\mathbf{K}_\Sigma = \mathbf{K}$ is called *Wittich's matrix*. $\mathbf{K}$, $\mathbf{y}$, and $\mathbf{t}$ can be brought to the form

$$\mathbf{P}\mathbf{K}\mathbf{P}^T = \begin{pmatrix} \mathbf{0} & -\mathbf{L}^T \\ \mathbf{L} & \mathbf{0} \end{pmatrix}, \quad \mathbf{P}\mathbf{y} = \begin{pmatrix} \mathbf{y}'' \\ \mathbf{y}' \end{pmatrix}, \quad \mathbf{P}\mathbf{t} = \begin{pmatrix} \mathbf{t}'' \\ \mathbf{t}' \end{pmatrix}$$

by permuting columns and rows, simultaneous in such a way that all even indexed ones come before all odd indexed ones. Then $\mathbf{P}\mathbf{K}\mathbf{P}^T$ is a consistently ordered weakly cyclic matrix of index 2, and—as pointed out by Niethammer [22]—we may apply the *nonlinear SOR method* to (1.1):

$$\begin{aligned} \mathbf{y}''_{m+1} &:= -\omega \mathbf{L}^T \log \rho(\mathbf{t}' + \mathbf{y}'_m) + (1-\omega)\mathbf{y}''_m, \\ \mathbf{y}'_{m+1} &:= \omega \mathbf{L} \log \rho(\mathbf{t}'' + \mathbf{y}''_{m+1}) + (1-\omega)\mathbf{y}'_m, \end{aligned} \qquad m = 0, 1, 2, \cdots.$$

* Received by the editors January 24, 1980, and in revised form February 22, 1982.

† Seminar für Angewandte Mathematik, Eidgenössische Technische Hochschule Zürich, CH-8092 Zürich, Switzerland. This work is part of a thesis submitted for Habilitation at Eidgen. Tech. Hochschule, Zürich, Switzerland.

($\mathbf{y}_0'$, $\mathbf{y}_0''$, and the relaxation factor ω must be given.) As shown both by the author [11] and by Hübner [16], each iteration step still requires only $O(N \log N)$ operations.

In [12] we established new theoretical results on this and several other iterative methods for solving (1.1), namely the *nonlinear Jacobi iteration* with relaxation (JOR)

$$\mathbf{y}_{m+1} := \omega\Phi(\mathbf{y}_m) + (1-\omega)\mathbf{y}_{m-1}, \qquad m = 0, 1, 2, \cdots$$

($\mathbf{y}_0$ and ω given), a *nonlinear second order Euler iteration*

$$\mathbf{y}_{m+1} := \omega\Phi(\mathbf{y}_m) + (1-\omega)\mathbf{y}_{m-1}, \qquad m = 0, 1, 2, \cdots$$

($\mathbf{y}_0 = \mathbf{y}_{-1}$ and ω given), the related *nonlinear Chebyshev iteration* (CSI) using an ω depending on m, and the *nonlinear cyclic Chebyshev iteration* (CCSI) so related to SOR. Both SOR and CSSI require $\mathbf{K}_\Sigma = \mathbf{K}$, while the other methods allow other discretization (i.e., approximation) techniques.

The main purpose of this paper is to present numerical experiments with SOR, JOR, and Euler iteration, the latter with various types of approximation. We also discuss some related questions that turn out to be important in practice, such as the use of a continuation method to avoid convergence to useless solutions of (1.1), the evaluation of the approximate mapping function and its derivative, the behavior of the boundary correspondence function θ at a corner of Γ in case Γ is piecewise analytic, and the elimination of corners by preliminary maps.

Our numerical experiments on the rate of convergence indicate that the range of application of our results in [12] is far wider than one would expect from the theory. Most theorems in [12] require either assumption (D) or assumption (SD)—as we called them—which could be replaced by the following more convenient conditions:

Assumption (D′): ρ is continuously differentiable.

Assumption (SD′): Γ is symmetric about the real axis and ν-fold rotationally symmetric about 0, where $\nu \geqq 1$ is a divisor of N; ρ is weakly monotone and continuously differentiable in $(0, \pi/\nu)$.

Moreover, we always assume that $\mathbf{y}^*$ is a solution of (1.1) and that, in case assumption (SD′) holds, both $\mathbf{y}^*$ and its initial approximation $\mathbf{y}_0$ (and thus all iterates $\mathbf{y}_m$) lie in the $(N/\nu - 1)$-dimensional subspace $\mathcal{S}$ of vectors $\mathbf{y} \in \mathbb{R}^{2N}$ satisfying

$$y_0 = y_N = 0, \qquad y_k = -y_{2N-k} \qquad (k = 1, \cdots, N-1), \tag{1.2a}$$

$$y_k = y_{k+2N/\nu} \qquad (k = 0, \cdots, 2N - 2N/\nu - 1 \text{ if } \nu > 1). \tag{1.2b}$$

(The existence of $\mathbf{y}^*$ was established in [10], [16].) Consequently, (D′) implies (D), while (SD′) and the additional conditions $\mathbf{K}_\Sigma = \mathbf{K}$ and

$$\theta_k := t_k + y_k \in (0, \pi/\nu), \qquad k = 1, \cdots, N/\nu - 1, \tag{1.3}$$

for $\mathbf{y} = \mathbf{y}^*$ imply (SD).

The classical discretization [4], [12] of Theodorsen's integral equation, where $\mathbf{K}_\Sigma = \mathbf{K}$ is Wittich's matrix, is based on interpolating the data $(\mathbf{t}, \mathbf{x})$, i.e.,

$$t_k := k\pi/N, \qquad x_k := \log \rho(t_k + y_k), \qquad k = 0, \cdots, 2N-1, \tag{1.4}$$

by a trigonometric polynomial T and evaluating the conjugate polynomial KT at every t_k, two operations done by a fast Fourier transform (FFT) [11], [15]. As we show in [13], [34], it does not cost much more to interpolate or approximate the data (1.4) (or rather its periodic extension) by a function $P\mathbf{x}$, where $P: \Pi_{2N}^R \to \mathcal{A}$ is an operator with known attenuation factors $\boldsymbol{\tau} = (\tau_k)_{k=-\infty}^{\infty} \in l_1$ [7], [13]. Here, $\mathcal{A}$ denotes the space of real 2π-periodic functions having absolutely converging Fourier series,

and Π_{2N}^R (Π_{2N}) is the space of $2N$-periodic real (complex) sequences. If we further denote the $2N$-point discrete Fourier transform (DFT) [3], [15] by $\mathscr{F}_{2N}: \Pi_{2N} \to \Pi_{2N}$, then the DFT coefficients $\mathbf{c} := \mathscr{F}_{2N}\mathbf{x}$ of $\mathbf{x}$ and the usual Fourier coefficients $\mathbf{C} := \mathscr{F}\mathbf{P}\mathbf{x}$ are related by $c_k = \tau_k C_k (\forall k)$ [7]. In particular, interpolation by periodic spline functions of degree $2m-1$ ($m \geqq 1$), which is of this type, proved to be optimal (both in the sense of Sard and Schoenberg and in the sense of Golomb and Weinberger) for data corresponding to values of functions $X \in H^m$, where

$$H^m := \{X \in C^{m-1}(\mathbb{R}, \mathbb{R}) : X \ 2\pi\text{-periodic}, d^{m-1}X/dt^{m-1} \text{ abs. cont.}, d^m X/dt^m|_{[0,2\pi]} \in L_2[0, 2\pi]\}. \tag{1.5}$$

We also allow for various classes of smoothed approximants such as trigonometric polynomials with Cesaro (Fejér) or with Lanczos smoothing and splines interpolating smoothed data (so-called smoothing by spline functions) [13].

To account for these modifications algebraically, we have to replace Wittich's matrix $\mathbf{K}$ by $\mathbf{K}_\Sigma := \mathbf{K}\boldsymbol{\Sigma}$, where $\boldsymbol{\Sigma}$ is a symmetric circulant Toeplitz matrix, for which $\|\mathbf{K}_\Sigma\| \leqq \|\boldsymbol{\Sigma}\| \leqq 1$, but very close to 1, in all cases of interest. Moreover, one can then replace

$$\varepsilon_\rho := \operatorname*{ess\,sup}_{0 \leqq \tau \leqq 2\pi} \left| \frac{\rho'(\tau)}{\rho(\tau)} \right|$$

by $\varepsilon := \varepsilon_\rho \|\mathbf{K}_\Sigma\|$ when choosing the relaxation factor ω (of one of the nonlinear iterative methods mentioned) according to the formulas given in [12] for the case when assumption (SD) is satisfied. Here we use these formulas even for asymmetric regions, and we always identify ε and ε_ρ, i.e., we neglect that $\|\mathbf{K}_\Sigma\|$ may be slightly smaller than $\|\mathbf{K}\|$, which equals 1.

Our experiments on the accuracy of the approximate mapping function show that the classical Theodorsen method (where $\mathbf{K}_\Sigma = \mathbf{K}$) becomes inaccurate if Γ is not smooth. Often the components of $\boldsymbol{\theta} := \mathbf{t} + \mathbf{y}$ are no longer monotone. Although more suitable types of approximation yield much more useful results, it seems that the best idea is to eliminate the corners by preliminary maps. If the resulting boundary is not starlike or if its ε_ρ is large, one can try additional preliminary maps such as, e.g., those incorporated in osculation methods [2], [4], [8], [14], [26]. Apparently, such preliminary maps were used successfully in the precomputer era of conformal mapping, but experiments with a sufficiently flexible computer program for an osculation method have only recently been published by Grassmann [8]. For Example 5.2 (below), his program has been linked with a new general program to eliminate corners.

If Γ is smooth, the discrete Theodorsen equation can also be solved by a combination of Newton's method [4, p. 90] with a linear iterative method, e.g., by Newton–SOR [22], or by Newton–Euler. Though these methods are not treated explicitly here or in [12], it is clear from the general theory [23] that their asymptotic behaviors are similar to those of the corresponding nonlinear iterative methods. They are particularly efficient if the evaluation of ρ is expensive and that of ρ' is not much more expensive.

There are also a number of *related numerical methods* [4, pp. 105–115], [31], [33], for computing the conformal map of the disk D onto the given region Δ. They are all based on the fact that $t \mapsto Y(t) := \operatorname{Im} G(e^{it})$ is the conjugate periodic function KX of $t \mapsto X(t) := \operatorname{Re} G(e^{it})$ if G is analytic in D, continuous in $\bar{D}$, and real valued at 0. (There are also a great number of numerical methods for the inverse map.) If we let $G(w)$ be a suitable branch of $\log [g(w)/w]$, the relation $Y = KX$ becomes

$$\operatorname{Im} \log \{e^{-it} g(e^{it})\} = K[\operatorname{Re} \log \{e^{i\cdot} g(e^{i\cdot})\}](t), \tag{1.6}$$

and in view of (1.0) this leads easily to Theodorsen's integral equation

$$\theta(t) - t = K[\log \rho(\theta(\cdot))](t) \qquad (\forall t \in \mathbb{R}). \tag{1.7}$$

(1.7) is obviously restricted to starlike regions Δ, but one must be aware that relation (1.6) persists if this property does not hold. If we assume that $\Gamma = \{\zeta(\sigma); 0 \leqq \sigma \leqq 1\}$, relation (1.6) in conjunction with the condition $g(e^{it}) = \zeta(\theta(t))$ defining θ becomes upon discretization a nonlinear system of equations for $\theta(t)$. Similarly, one could use $G(w) = g(w)/w$, as in the method of Kulisch and Melentjew [4, pp. 106–109], or $G(w) = g(w)$ as in the methods of Fornberg [33], and Chakravarthy and Anderson [31], or even $G(w) = \log g'(w)$ as basically in the methods of Timman [4, pp. 110–111], Woods [39], James [35], Bauer, Garabedian, Korn, and Jameson [30], which were designed for mapping the exterior of an airfoil profile and allow for an open trailing edge [30], [35], [39] and for various other less idealized situations [35], [39, p. 302]. In all these cases one can apply the FFT. (This was in fact done in [30], [33].)

The discretized Theodorsen equation is particularly simple since it is in a natural way a fixed point equation of a function which is a contraction if $\varepsilon < 1$. Even for $\varepsilon \geqq 1$ the various methods to solve it are well understood if assumption (SD) holds [12]. This is not really true for any of the other methods mentioned.[1] Its drawback—the limitation to starlike domains—can be overcome in practice by preliminary maps, cf. §§ 4 and 5. Among the more recent methods, the one in [31] is not competitive since conjugation is done extremely inefficiently there. (The matrix $\mathbf{A}$ in [31] could be replaced by our $\mathbf{L}$ defined above, and multiplication by $\mathbf{L}$ is an $O(N \log N)$ operation [11].) In contrast, the methods in [30] and [33] are also "fast". They require that Γ be smooth. The first one has the advantage that the derivative of the approximate mapping function never vanishes. Fornberg [33] chooses $G(w) = g(w)$ and solves the nonlinear system (mentioned above) in the frequency domain, i.e., by requiring that the Fourier coefficients of $X + iY$ with negative index vanish. Apart from his different choice for G he determines in principle the same approximate mapping function as we do by solving (1.1) with $\mathbf{K}_\Sigma = \mathbf{K}$, or, generally, the correspondingly discretized version of (1.6). Therefore, our discussion of accuracy in § 7 is also relevant to Fornberg's method and to some of the other methods. (In fact, only a small part of our material is strictly limited to Theodorsen's equation.) It is still an open question which method is best in which situation. But the numerical experiments presented here show that our methods are definitely among the fastest.

2. Numerical experiments on the rate of convergence. The underrelaxation factors $\omega^*(\varepsilon)$ given in [12] for JOR, SOR, and Euler iteration are optimal in the following sense: If assumption (D′) holds and the spectrum of $\mathbf{J} := \mathbf{\Phi}'(\mathbf{y}^*)$ (known to satisfy $\Lambda(\mathbf{J}) \leqq \varepsilon$) is purely imaginary and contains $\pm i\varepsilon$, or if assumption (SD′) holds (possibly up to the monotonicity of ρ) and the spectrum of the restriction $\mathbf{J}|_{\mathcal{S}}$ of $\mathbf{J}$ to $\mathcal{S}$ has these properties, then the spectral radius $\Lambda(\mathbf{J}_\omega)$ of the Fréchet derivative of the respective (nonlinear) iteration function becomes minimal for $\omega = \omega^*$. This means that ultimately the rate of convergence becomes best for $\omega = \omega^*$ (if $\mathbf{y}_m \to \mathbf{y}^*$ at all). Practically, it is important to know whether ω^* is still a good choice if some of these conditions do not hold. In [12] we proved that the spectrum of $\mathbf{J}|_{\mathcal{S}}$ is purely imaginary if $\mathbf{K}_\Sigma = \mathbf{K}$ and (SD′) and (1.3) hold; but we must expect that actually $\Lambda(\mathbf{J}|_{\mathcal{S}}) < \varepsilon$.

[1] However, a new theoretical understanding of Fornberg's method arises from recent results presented by O. Widlund at the Workshop on Computational Problems in Complex Analysis at Stanford (September 1981).

Moreover, we need a starting vector $\mathbf{y}_0$ so that $\mathbf{y}_m \to \mathbf{y}^*$. Many questions may be raised: Is $\mathbf{y}_0 = 0$ good enough? And, if $\mathbf{y}_m \to \mathbf{y}^*$, are we sure that $\mathbf{y}^*$ is a useful solution? How fast is the convergence at the beginning compared with the asymptotic convergence rate?

In this section we describe a few of our experiments with the nonlinear JOR, SOR, and Euler iterations. We gradually relax assumption (SD'). Fortunately, it turns out that the convergence behavior is not much affected.

Experiments with the nonlinear cyclic Chebyshev semi-iteration (CCSI) and with the Chebyshev semi-iteration (CSI) showed that they are usually slightly less efficient than SOR and Euler iteration, respectively. In particular, the first few iterations often yield only a moderate improvement. But there are also examples where CCSI or CSI reach the stopping criterion within fewer iterations.

Example 2.1. The reflected ellipse

$$\rho(\tau) := [1-(1-\alpha^2)\cos^2\tau]^{1/2} \qquad (0<\alpha\leqq 1) \tag{2.1}$$

obtained by reflecting an ellipse with semiaxes $1/\alpha$ and 1 across the unit circle satisfies assumption (SD') with $\nu = 2$. Its exact boundary correspondence function is elementary,

$$\theta(t) = \tan^{-1}(\alpha \tan t), \tag{2.2}$$

and, owing to the fast convergence of the Fourier series of $Y(t) = \theta(t) - t$, high-accuracy results may be obtained with moderate N (unless α is small). These two features also explain the popularity of this example [4], [21], [22], [28].

Some of our results are summarized in Tables 2.1 and 2.2. Except for the last two lines of Table 2.2, a total of $2N = 64$ boundary points have been computed, but due to the symmetries, the number of variables was only 16 (for JOR and Euler) or 32 (for SOR). In addition to $\varepsilon = \frac{1}{2}(1-\alpha^2)/\alpha$, $\omega^* := \omega^*(\varepsilon)$, and the corresponding asymptotic factor of convergence σ^*, we list in Table 2.1 the actual spectral radius $\Lambda(\mathbf{J})$ of $\mathbf{J}$, the true optimal relaxation factor $\omega^{\text{opt}} := \omega^*(\Lambda(\mathbf{J}))$, and the corresponding asymptotic convergence factor σ^{opt}. The subscripts J and S refer to JOR and SOR iteration, respectively. Recall that for the Euler iteration $\omega_E^*(\varepsilon) = \omega_S^*(\varepsilon)$ and $\sigma_E^*(\varepsilon) = [\sigma_S^*(\varepsilon)]^{1/2}$, cf. [12, Thm. 6.2]. Finally, we display

$$i^* := -1/\log_{10}\sigma^*, \tag{2.3}$$

i.e., the number of iterations ultimately needed to get one additional decimal of the result if σ^* were the correct asymptotic factor of convergence. This may be compared in Table 2.2 with the number

$$m(l) := \inf\{m : \|\mathbf{y}_m - \Phi(\mathbf{y}_m)\|_\infty \leqq 10^{-l}\} \tag{2.4}$$

TABLE 2.1
Comparison of nearly optimal and optimal underrelaxation (Ex. 2.1).

α	ε	$\Lambda(\mathbf{J})$	ω_J^*	ω_J^{opt}	σ_J^*	σ_J^{opt}	ω_S^*	ω_S^{opt}	σ_S^*	σ_S^{opt}	i_J^*	i_S^*
.8	.225	.221	.952	.954	.220	.215	.988	.988	.0123	.0119	1.52	.524
.6	.533	.523	.779	.785	.471	.464	.937	.940	.0625	.0604	3.06	.830
.4	1.050	1.030	.476	.485	.724	.717	.816	.821	.184	.179	7.13	1.36
.3	1.517	1.488	.303	.311	.835	.830	.710	.716	.290	.284	12.75	1.86
.2	2.400	2.354	.148	.153	.923	.920	.556	.562	.444	.438	28.77	2.84
.1	4.950	4.549	.039	.047	.980	.979	.331	.354	.669	.646	115.12	5.74
.05	9.975	9.783	.010	.010	.995	.995	.181	.185	.819	.815	460.52	11.50

TABLE 2.2
Actual convergence of JOR, SOR, *and Euler iteration* (*Ex.* 2.1).

N	α	$m_J(3)$	$m_J(6)-m_J(3)$	r_J	e_J
32	.8	3	4	$7.87_{10^{-7}}$	$1.45_{10^{-7}}$
	.6	6	9	$7.35_{10^{-7}}$	$3.18_{10^{-7}}$
	.4	17	20	$8.00_{10^{-7}}$	$3.70_{10^{-7}}$
	.3	30	37	$8.52_{10^{-7}}$	$2.71_{10^{-6}}$
	.2	75	78	$9.83_{10^{-7}}$	$1.14_{10^{-4}}$
	.1	311	317	$8.99_{10^{-7}}$	$6.63_{10^{-3}}$
128	.2	77	82	$8.85_{10^{-7}}$	$3.38_{10^{-7}}$
	.1	331	324	$9.32_{10^{-7}}$	$2.44_{10^{-7}}$
N	α	$m_S(3)$	$m_S(6)-m_S(3)$	r_S	e_S
32	.8	2	2	$5.26_{10^{-9}}$	$3.29_{10^{-10}}$
	.6	3	3	$8.26_{10^{-8}}$	$4.79_{10^{-9}}$
	.4	5	4	$3.42_{10^{-7}}$	$8.95_{10^{-8}}$
	.3	7	5	$7.31_{10^{-7}}$	$2.68_{10^{-6}}$
	.2	10	9	$9.86_{10^{-7}}$	$1.14_{10^{-4}}$
	.1	[31]	[23]	$8.86_{10^{-7}}$	1.12
128	.2	11	8	$8.15_{10^{-7}}$	$3.92_{10^{-7}}$
	.1	[34]	[45]	$6.33_{10^{-7}}$	1.60
N	α	$m_E(3)$	$m_E(6)-m_E(3)$	r_E	e_E
32	.8	3	3	$2.35_{10^{-7}}$	$2.68_{10^{-8}}$
	.6	5	5	$3.32_{10^{-7}}$	$8.13_{10^{-8}}$
	.4	8	8	$8.67_{10^{-7}}$	$2.58_{10^{-7}}$
	.3	12	11	$8.48_{10^{-7}}$	$2.98_{10^{-6}}$
	.2	19	18	$8.22_{10^{-7}}$	$1.14_{10^{-4}}$
	.1	[59]	[46]	$9.15_{10^{-7}}$	1.12
128	.2	20	17	$9.44_{10^{-7}}$	$4.90_{10^{-7}}$
	.1	[∞]		1.91	

of iterations actually needed to satisfy the discrete Theodorsen equation to within a maximum error of 10^{-l} with the JOR (m_J), the SOR (m_S), or the Euler iteration (m_E). Here, $\mathbf{y}_0 = \mathbf{0}$ throughout. Brackets $[\cdot]$ indicate that the resulting vector $\boldsymbol{\theta}_{m(l)+1} := \mathbf{t} + \mathbf{y}_{m(l)+1}$ does not satisfy (1.3). We also list the residual $r = r(m(6))$ generally defined by

$$r(m) := \|\mathbf{y}_m - \boldsymbol{\Phi}(\mathbf{y}_m)\|_\infty. \tag{2.5}$$

(So, $r(m(l)) \leqq 10^{-l}$ by definition.) Finally, $e = e(m(6)+1)$ is the actual error

$$e(m) := \|\mathbf{y}_m - Y(\mathbf{t})\|_\infty \tag{2.6}$$

of the next iterate. (Since the evaluation of $\boldsymbol{\Phi}$ needed in (2.4) adds to the cost, one is inclined to finish the $(m(l)+1)$st step that is in progress.)

Table 2.1 shows that the differences between ε and $\Lambda(\mathbf{J})$, between ω^* and ω^{opt}, and between σ^* and σ^{opt} are small and cannot affect the convergence essentially. Comparing $m(3)$ in Table 2.2 with $3i^*$, we note that at the beginning the JOR iteration is more effective, while the SOR iteration is slightly less effective than suggested by the corresponding asymptotic rate. Nevertheless, SOR is faster than JOR and Euler even at the beginning, and even in the case of small ε. Later its superiority is out of

the question: as predicted by the theory, it then converges twice as fast as Euler, which is itself much faster than JOR.

Surprisingly, for $\alpha = .1$ ($\varepsilon = 4.950$) the JOR method still yields a reasonable solution with $e_J(629) \doteq 8.99 \times 10^{-7}$, while both SOR and Euler converge to a solution violating (1.3) and with an error of about 1.12. Since the difference between r and e shows that the discretization error becomes important when $\alpha \leqq .3$, one might hope—at least if the JOR result were not known—that replacing $N = 32$ by $N = 128$ would lead to a better solution. However, while e_J, e_S, and e_E become in fact essentially smaller for $\alpha = .2$, the SOR iteration still converges for $\alpha = .1$ to a useless solution, and the Euler iteration does not converge at all. An inspection of the Euler data reveals that the odd indexed and the even indexed iterates converge to different limits. So, we actually get a solution of system (5.12) in [12],

$$\mathbf{y}^{(1)} = \boldsymbol{\Phi}(\mathbf{y}^{(2)}), \qquad \mathbf{y}^{(2)} = \boldsymbol{\Phi}(\mathbf{y}^{(1)}), \tag{2.7}$$

which has double size. As we noted there, Euler's iteration is equivalent to an SOR iteration for (2.7); and (2.7) may have solutions $\mathbf{y}^{(1)} \neq \mathbf{y}^{(2)}$ that do not satisfy $\mathbf{y} = \boldsymbol{\Phi}(\mathbf{y})$. In fact, here $\|\mathbf{y}^{(1)} - \mathbf{y}^{(2)}\|_\infty = r_E(\infty) \doteq 1.91$.

We also note that in the three cases where $\boldsymbol{\theta}_{m(l)}$ violates (1.3), the convergence is definitely slower than predicted by i^*. So, the eigenvalues of $\mathbf{J}|_{\mathscr{S}}$ are probably no longer purely imaginary. At least, this is motivated by

LEMMA 1. *Suppose that either assumption* (D′) *or assumption* (SD′) *holds except that ρ may be nonmonotone. Assume further that* $\mathbf{J}$ *or* $\mathbf{J}_{\mathscr{S}}$, *respectively, has purely imaginary eigenvalues, and that the iterates* $\mathbf{y}_m$ *created by the nonlinear* SOR *method converge to* $\mathbf{y}^*$. *Finally, let* $\sigma := \sigma_S^*(\Lambda(\mathbf{J}^S))$ *or* $\sigma_S^*(\Lambda(\mathbf{J}^S|_{\mathscr{S}}))$, *respectively, where* $\sigma_S^*(\Lambda) := \Lambda^2/[1+(1+\Lambda^2)^{1/2}]^2$ (*cf.* [12, *Thm.* 5.1]). *Then in any norm*

$$\limsup_{m\to\infty} \frac{\|\mathbf{y}_m - \mathbf{y}^*\|}{\|\mathbf{y}_{m-1} - \mathbf{y}^*\|} \geqq \limsup_{m\to\infty} \|\mathbf{y}_m - \mathbf{y}^*\|^{1/m} = \sigma, \tag{2.8a}$$

$$\limsup_{m\to\infty} \frac{\|\mathbf{y}_{m+1} - \mathbf{y}_m\|}{\|\mathbf{y}_m - \mathbf{y}_{m-1}\|} \geqq \limsup_{m\to\infty} \|\mathbf{y}_{m+1} - \mathbf{y}_m\|^{1/m} = \sigma. \tag{2.8b}$$

The same relations hold for the nonlinear Euler iteration if σ is replaced by $\sigma^{1/2}$.

Proof. The inequality in (2.8a) is just [23, Statement 9.3.1]. The equality at right is established as [23, Statement 10.1.4]; additionally, one has to take into account that all eigenvalues of $\mathbf{J}_\omega^S$ have moduli $\sigma = \Lambda(\mathbf{J}_\omega^S)$. In case of assumption (SD′), only the restrictions to $\mathscr{S}$ must be considered [12]. A further inspection of the proofs in [23] shows that (2.8b) also holds, since $\mathbf{J}_\omega^S$ is a strong F-derivative if ρ is continuously differentiable [23]. For Euler's iteration, $(\mathbf{J}_\omega^E)^2 = \mathbf{J}_\omega^S$ [12]. □

Example 2.2. Let Γ consist of the right half of the reflected ellipse (2.1) and of the left half of the ellipse

$$\rho(\tau) = [1 - (1-\alpha^2)\cos^2\tau]^{-1/2} \tag{2.9}$$

with semiaxes α and 1. Assumption (SD′) is nearly satisfied with $\nu = 1$ except that ρ is not monotone. The question is whether this affects the asymptotic rate of convergence. As an indicator we determine

$$q(l) := \left[\frac{\|\mathbf{y}_{m(l)+1} - \mathbf{y}_{m(l)}\|_2}{\|\mathbf{y}_{m(l-1)+1} - \mathbf{y}_{m(l-1)}\|_2}\right]^{1/[m(l)-m(l-1)]}, \tag{2.10}$$

which may be considered as an approximate upper bound for $\Lambda(\mathbf{J}_\omega^S|_{\mathscr{S}})$ or $\Lambda(\mathbf{J}_\omega^E|_{\mathscr{S}})$, respectively, if $\mathbf{J}|_{\mathscr{S}}$ has purely imaginary eigenvalues. ((2.8b) suggests that one compute

$\|\mathbf{y}_{m+1}-\mathbf{y}_m\|_2^{1/m}$ instead, which usually turns out to be larger than $q(l)$, however.) From our experiments with $N=128$ and $\mathbf{y}_0=\mathbf{0}$, we list, on the top three lines of Table 2.3, $q_S(6)$, $q_E^T(6)$, and $q_E^{S3}(6)$, where the superscripts T and S3 denote trigonometric and cubic spline interpolation [13, Ex. 5.1], respectively. Note that q is close to the corresponding σ^* except for $\alpha=0.2$ ($\varepsilon=2.4$), where the SOR solution and the Euler solution with trigonometric interpolation (E/T) yield a solution $\boldsymbol{\theta}$ satisfying (1.3) but having nonmonotone components indicated by braces $\{\cdot\}$. In contrast, third degree spline interpolation (E/S3) leads to a more useful solution.

TABLE 2.3
Convergence in case of a symmetric region with nonmonotone ρ (Ex. 2.2) and in case of an asymmetric region (Ex. 2.3).

Ex.	α	σ_S^*	$m_S(6)$	$q_S(6)$	σ_E^*	$m_E^T(6)$	$q_E^T(6)$	$m_E^{S3}(6)$	$q_E^{S3}(6)$
2.2	.8	.01235	4	.01235	.11111	6	.11114	6	.11113
	.4	.18367	9	.18742	.42857	18	.42897	18	.41575
	.2	.44444	{24}	.48569	.66667	{47}	.70880	39	.68274
2.3	.8	.01235	4	.01282	.11111	6	.11377	6	.11377
	.4	.18367	10	.18580	.42857	19	.42618	20	.42057
	.2	.44444	23	.54849	.66667	44	.70252	43	.66878

Example 2.3. Let Γ consist of the left half of the unit circle, of the part of the reflected ellipse (2.1) in the first quadrant, and of the part of the ellipse (2.9) in the fourth quadrant. So, Γ is again a piecewise analytic curve with straight angles, but now it is asymmetric. Nevertheless, we use $\omega=\omega^*(\varepsilon)$ as defined for symmetric curves. Results are listed on the lower three lines of Table 2.3. ($N=128$ and $\mathbf{y}_0=\mathbf{0}$ again.) Here, the components of $\boldsymbol{\theta}_{m(6)}$ are always monotone, and only $q_S(6)$ in the case $\alpha=.2$ indicates a slower convergence. Yet, $q_E^T(6)$ turns out to be close to σ_E^*, although the iterates tend to the same solution as with the SOR method. On the other hand, $q_S(9)\doteq .38048$, and an experiment with an alternate starting point than $\mathbf{y}_0=\mathbf{0}$ yields $q_S(6)\doteq .49168$, $q_S(9)\doteq .38513$. We must conclude that in some examples $q(l)$ is not a reliable estimate of $\Lambda(\mathbf{J}_\omega)$.

Example 2.4. A square with the center at the origin satisfies assumption (SD'). As we will see in § 7 trigonometric interpolation of $\log\rho(\mathbf{t}+\mathbf{y}^*)$ leads to an approximate mapping function g_N for which $g_N(\partial D)$ has ripples. We use this example to demonstrate other approximation techniques. In addition to the trigonometric interpolation (T), we consider Cesàro (C) and Lanczos (L) smoothing [13, Ex. 6.1], interpolation by a first degree spline [13, Ex. 5.1], and smoothing by a first degree and by a cubic spline, both with smoothing parameter $\tilde{\rho}=10^4$ (S1/10^4 and S3/10^4) [13, Ex. 6.2]. See Table 2.4. Surprisingly, the data $m(6)$, $r(m(6))$, and $q_E(m(6))$ are nearly the same in all cases except for trigonometric interpolation, where it takes one iteration more to satisfy

TABLE 2.4
Convergence of iterates based on various types of approximation (Ex. 2.4).

	T	C	L	S1	S1/10^4	S3/10^4
$m(6)$	15	14	14	14	14	14
$r(m(6))\times 10^6$	.51198	.42876	.43405	.43412	.43353	.43272
$q_E(6)$	.41854	.41404	.41416	.41418	.41420	.41331

the stopping criterion $r(m(6)) \leqq 10^{-6}$ and where $r(m(6))$ is nevertheless larger than for the other five.

To enable the reader to estimate the computing time of any of the examples we list in Table 2.5—as a function of N—the time (in seconds) for *one* JOR or Euler iteration step with the boundary function $\rho(\tau) = \exp(\alpha \cos \beta\tau)$. For comparison we measured this time also when **Kx** was computed by multiplication with Wittich's matrix—as suggested in earlier texts—instead of by applying the FFT. In both cases it is possible to take advantage of symmetries, cf. [11]. The last two columns show the time for one step with axial symmetry.

TABLE 2.5
Computing time for one JOR *or one Euler iteration step (seconds on* CDC 6400/6500).

N	no symmetry		axial symmetry	
	Wittich	FFT	Wittich	FFT
16	.03	.04	.02	.02
32	.09	.08	.05	.04
64	.30	.15	.16	.08
128	1.04	.31	.55	.16
256	3.72	.64	2.08	.34
512	14.06	1.34	8.04	.69
1,024	54.41	2.79	31.05	1.46
2,048		6.02		3.00

(These execution times have been measured on the CDC 6400/6500 at Eidgen. Tech. Hochschule, Zurich, where an addition or subtraction takes 1.1 μsec and a multiplication or division, 5.7 μsec. The FFT program used here was a general purpose ALGOL60 implementation of the radix-2 algorithm and thus not most efficient for conjugation, where permutation of data to reverse binary order could be omitted. Most of our other experiments were done instead with a hand-optimized version of Singleton's FORTRAN mixed radix FFT program [24], which proved to be essentially faster in case N is a large power of 2.)

These execution times are hardly affected if **K** is replaced by a more general conjugation process $\mathbf{K}_\Sigma$, but the preparations may cause some overhead (cf. [13]).

The computing time for one SOR iteration is essentially the same too if the program published in [11] is used for the conjugation; however, one cannot capitalize on axial symmetry easily.

3. Continuation methods. There is strong experimental evidence that even for quite simple boundaries Γ and a suitable N, the discrete Theodorsen equation (1.1) may have more than one solution. In this section we state conditions assuring the existence of a unique special solution, which is also the only reasonable one. This solution is obtained from the unique solution for $\Gamma = \partial D$ (viz., $\mathbf{y}^* = \mathbf{0}$) by a homotopy. Practically, it can therefore be computed by means of a continuation method [23, pp. 230–234]. For the theory we either need assumption (D′) or assumption (SD′).

Under assumption (D′) we consider the following initial value problem:

$$\mathbf{y}'(\eta) = [\mathbf{I} - \eta\Phi'(\mathbf{y}(\eta))]^{-1}\Phi(\mathbf{y}(\eta)), \tag{3.1a}$$

$$\mathbf{y}(0) = \mathbf{0}. \tag{3.1b}$$

If we assume that $\mathbf{I}-\eta\Phi'(\mathbf{y}(\eta))$ remains regular for $0 \leqq \eta < \eta_0$, it is easy to conclude that the solution of (3.1) exists there, is continuously differentiable and satisfies

$$\mathbf{y}(\eta) = \eta\Phi(\mathbf{y}(\eta)), \tag{3.2a}$$

i.e.,

$$\mathbf{y}(\eta) = \mathbf{K}_\Sigma \log \rho^\eta(\mathbf{t}+\mathbf{y}(\eta)), \tag{3.2b}$$

cf. [23, p. 233]. (In fact, (3.1a) is obtained by differentiating (3.2a).) So, $\mathbf{y}(\eta)$ is the solution of the discrete Theodorsen equation corresponding to the boundary Γ_η with the polar coordinates τ, $\rho^\eta(\tau)$. In particular, if $\eta_0 > 1$, $\mathbf{y}(1)$ is a solution of the given equation (1.1).

By [12, Thm. 3.1], we know that $\mathbf{y}(\eta)$ is the only solution of (3.2) as long as $\eta \in [0, 1/\varepsilon)$. Along the path $\eta \mapsto \mathbf{y}(\eta)$ this solution can be continued uniquely until $\mathbf{I}-\eta\Phi'(\mathbf{y}(\eta))$ becomes singular. This does not exclude the existence of other solutions in case $1/\varepsilon \leqq \eta < \eta_0$, nor does it guarantee the monotonicity of the components of $\boldsymbol{\theta}(\eta) := \mathbf{t}+\mathbf{y}(\eta)$.

Under assumption (SD'), $\Phi(\mathcal{S}) \subset \mathcal{S}$ (cf. [12, App. 2]). If $\mathbf{y} \in \mathcal{S}$ satisfies (1.3) and if $\mathbf{K}_\Sigma = \mathbf{K}$, the eigenvalues of $\Phi'(\mathbf{y})|_{\mathcal{S}}$ are purely imaginary [12, Thm. 3.4], and hence the restricted operator

$$[\mathbf{I}-\eta\Phi'(\mathbf{y})]|_{\mathcal{S}} \tag{3.3}$$

is regular and defines an automorphism of $\mathcal{S}$. Consequently, $\mathbf{y}(\eta) \in \mathcal{S}$, $0 \leqq \eta < \eta_0$, and the path $\eta \mapsto \mathbf{y}(\eta)$ is well defined as long as $\mathbf{y}(\eta)$ satisfies (1.3).

In this case of symmetry, Hübner [16] proposed to replace ρ by

$$\hat{\rho}(\tau) := \begin{cases} \rho(0) & \text{if } \tau \leqq 0, \\ \rho(\tau) & \text{if } 0 < \tau < \pi/\nu, \\ \rho(\pi/\nu) & \text{if } \tau \geqq \pi/\nu, \end{cases} \tag{3.4a}$$

when $\rho(t_k + y_k)$, $k = 0, \cdots, N/\nu$, is evaluated, while the other components of $\hat{\rho}(\mathbf{t}+\mathbf{y})$ are determined by symmetry. We let

$$\hat{\Phi}(\mathbf{y}) := \mathbf{K} \log \hat{\rho}(\mathbf{t}+\mathbf{y}) \qquad (\forall \mathbf{y} \in \mathcal{S}). \tag{3.4b}$$

By [12, App. 2, Lemma 2] $\hat{\Phi}'(\mathbf{y})|_{\mathcal{S}}$ has purely imaginary eigenvalues. By the general Theorem 5.3.9 in [23], the mapping $\mathbf{y} \mapsto \mathbf{y} - \eta\hat{\Phi}(\mathbf{y})$ is a homeomorphism of $\mathcal{S}$ (for fixed η); thus, exactly one point $\mathbf{y} = \hat{\mathbf{y}}(\eta)$ is mapped onto $\mathbf{0}$. This is an alternate proof of

THEOREM 2 (Hübner [16]). *The equation* $\mathbf{y} = \eta\hat{\Phi}(\mathbf{y})$ *has exactly one solution* $\hat{\mathbf{y}}(\eta)$. *If it satisfies* (1.3), *it is also a solution of* (3.2); *otherwise*, (3.2) *has no solution satisfying* (1.3).

Hübner's original proof is based on the above-mentioned Lemma 2 and Brouwer's fixed point theorem; it only requires that $\hat{\rho}$ be absolutely continuous, while we need $\hat{\rho}$ continuously differentiable in the above proof.

Of course, $\hat{\mathbf{y}}(\eta)$ satisfies (3.1) with Φ replaced by $\hat{\Phi}$. So, $\hat{\mathbf{y}}(1)$ could be computed by any standard numerical method for solving initial value problems. However, evaluating $\hat{\mathbf{y}}'$ would require calculating $\hat{\Phi}'$ (i.e. ρ'), and we do not consider such methods in this paper. Likewise, $\mathbf{y}(1)$ could be computed through solving (3.1) if $\mathbf{I}-\eta\Phi'(\mathbf{y}(\eta))$ is regular for $0 \leqq \eta \leqq 1$.

The following continuation method [23, § 10.4], which does not require evaluating ρ', is another simple means for computing $\mathbf{y}(1)$ or $\hat{\mathbf{y}}(1)$: Let

$$0 = \eta_0 < \eta_1 < \eta_2 < \cdots < \eta_I = 1 \tag{3.5}$$

be a partition of $[0, 1]$. Denote by $\Phi_{\omega,\eta}$ the iteration function defining one step of either the JOR, the SOR, or the Euler iteration applied to the fixed point equation $\mathbf{y} = \eta\Phi(\mathbf{y})$ (i.e., to the boundary Γ_η). Then, define the iterates $\mathbf{y}_{i,m}$ by

$$
\begin{aligned}
&\mathbf{y}_{1,0} := \mathbf{0}, \\
&\mathbf{y}_{i+1,0} := \mathbf{y}_{i,m_i+1}, \qquad i = 1, \cdots, I-1, \\
&\mathbf{y}_{i,m+1} := \Phi_{\omega^*(\varepsilon\eta_i),\eta_i}(\mathbf{y}_{i,m}), \qquad m = 0, \cdots, m_i, \quad i = 1, \cdots, I-1, \\
&\mathbf{y}_{I,m+1} := \Phi_{\omega^*(\varepsilon),1}(\mathbf{y}_{I,m}), \qquad m = 0, 1, 2, \cdots.
\end{aligned} \tag{3.6}
$$

If (SD′) holds, a variant 2 of this algorithm may be defined by our replacing ρ by $\hat{\rho}$ and $\mathbf{K}_\Sigma$ by $\mathbf{K}$, i.e., Φ by $\hat{\Phi}$. A general theorem by Avila [23, 10.4.1] and the theory in [12] yield

THEOREM 3. *Under assumptions* (SD′) *and* (D′), *there exist a partition* (3.5) *and integers* $m_1, \cdots, m_{I-1}$ *such that the variant* 2 *of algorithm* (3.6) *yields a sequence* $\{\mathbf{y}_{I,m}\}$ *converging to the fixed point* $\hat{\mathbf{y}}(1)$ *of* $\hat{\Phi}$.

Of course, if $\hat{\mathbf{y}}(\eta)$ satisfies (1.3) for $0 \leqq \eta \leqq 1$, we may as well use variant 1. Moreover, variant 1 proved practically useful even for asymmetric boundaries Γ. In any case one has to choose the partition (3.5) and the integers m_i somehow. A risky choice may lead to no solution or the wrong one; a too cautious choice is expensive.

Our experiments have been done with the following values, which depend on two parameters I_0 and l_0:

$$
\begin{aligned}
&I := \lfloor I_0\varepsilon \rfloor + 1, \qquad \eta_i := i/I, \\
&m_i := m_i(l_0) := \inf\{m : \|\mathbf{y}_{i,m} - \eta_i\Phi(\mathbf{y}_{i,m})\|_\infty \leqq 10^{-l_0}\}, \qquad i = 1, \cdots, I-1.
\end{aligned} \tag{3.7}
$$

Example 3.1. In Example 2.1 (cf. Table 2.2), we always obtain the unique fixed point of $\hat{\Phi}$ except when $\alpha = .1$, in which case SOR and Euler iteration applied to (1.1) converge to another fixed point of Φ, while the JOR method still yields the common fixed point of Φ and $\hat{\Phi}$. However, we can compute this fixed point now more efficiently with the continuation method (3.6) (variant 1 or 2) based on SOR or Euler. Table 3.1 shows for the SOR method with $N = 128$, variant 1 of (3.6), and the two problems with $\alpha = .1$ and $\alpha = .05$, respectively, the total number

$$
M_P := \sum_{i=1}^{I-1} [m_i(l_0) + 1] \tag{3.8}
$$

TABLE 3.1
Number of steps required by the continuation method (Ex. 3.1: reflected ellipse).

		$\alpha = .1$ ($\varepsilon = 4.950$)			$\alpha = .05$ ($\varepsilon = 9.975$)		
I_0	l_0	I	M_P	$M_P + m_S(6)$	I	M_P	$M_P + m_S(6)$
.5	1	3	[11]	46	5	[51]	[ ]
.5	2	3	16	51	5	[ ]	[ ]
.5	3	3	22	57	5	[ ]	[ ]
1	1	5	[17]	50	10	[45]	[124]
1	2	5	28	61	10	97	159
1	3	5	38	71	10	149	211
2	1	10	[27]	58	20	[65]	126
2	2	10	53	84	20	168	228
2	3	10	80	111	20	275	336

of evaluations of Φ required to determine the starting point $\mathbf{y}_{I,0}$ of the last secondary iteration in (3.6), and the total number $M_P + m_S(6)$ of steps done until $\mathbf{y}_{I,m}$ satisfies (2.4) with $l = 6$. For $\alpha = .1$ we always end up with the correct solution, although $\mathbf{y}_{I,0}$ violates (1.3) if $l_0 = 1$. However, if $\alpha = .05$ and $I_0 = .5$, the path $\mathbf{y}(\eta)$ is always left, and this still happens for $\alpha = .05$, $I_0 = 1$, $l_0 = 1$. On the other hand, in case of convergence to the correct solution, the number of steps required varies strongly.

Example 3.2. Theorem 2 does not apply to Example 2.2, and so there could exist another solution with monotone $\boldsymbol{\theta}$ in the case $\alpha = .2$ (cf. Table 2.3). However, our experiments with the continuation method have always delivered the same solution. Moreover, $N = 512$ and $\mathbf{y}_0 = \mathbf{0}$ immediately lead to a monotone $\boldsymbol{\theta}$ (see Ex. 7.2).

These two examples show that further investigations on the appropriate choice of N, I, the partition $\{\eta_i\}$ and the numbers m_i of secondary iterations are worthwhile. Ultimately one needs a programmable strategy containing feedback loops for the determination of these parameters.

4. The behavior of the boundary correspondence function at a corner of a piecewise analytic boundary. While many other constructive methods for conformal mappings [4] require that the boundary Γ be differentiable or need to be modified to allow for corners, Theodorsen's method is less restrictive (cf. [12, Thms. 4.3, 7.3]). To be sure, for some results on local convergence, we had to assume in [12] that ρ' exists (except at points on a symmetry axis). But as we pointed out, differentiability seems not to be crucial for the local convergence in practice. However, if the approximation of $\log \rho(\theta(t))$ is done by trigonometric interpolation, corners strongly infect the accuracy of the resulting approximate values of the boundary correspondence function θ. In order to select a more appropriate class of approximants, we cite some results on the behavior of θ. We restrict ourselves to the most important case, namely to a piecewise analytic boundary Γ.

Assume first that Δ is a Jordan region with $0 \in \Delta$ and a piecewise analytic boundary Γ. Let $g : \bar{D} \to \bar{\Delta}$ be the continuous extension of a conformal map with $g(0) = 0$, $g'(0) > 0$ of the unit disk D onto Δ. Denote by $\zeta_j := g(w_j)$, $j = 1, \cdots, J$, the corners (or, rather, the breakpoints), which are assumed to be regular points of the analytic arcs meeting there under the inner angles $\pi\alpha_j$, where $0 < \alpha_j \leqq 2$. Let $\zeta_0 = g(w_0)$ be any of these corners, $\pi\alpha$ the corresponding angle, and set $h := w - w_0$. Then, according to a theorem by Lehman [19] generalizing earlier work of Lichtenstein, Kellog, Warschawski, and Lewy, the following asymptotic expansion holds for $h \to 0$ if $\arg h$ remains bounded for some continuous branch of the argument:

$$\begin{aligned} g(w_0 + h) &\sim \zeta_0 + \sum_{k,l,m} a_{klm} h^{k+l\alpha} (\log h)^m \\ &= \zeta_0 + a_{010} h^{\alpha} + a_{111} h^{1+\alpha} \log h + a_{110} h^{1+\alpha} + O(h^{2\alpha}), \end{aligned} \tag{4.1}$$

where $a_{010} \neq 0$, and the sum runs over

$$k \geqq 0, \quad l \geqq 1, \quad m = 0 \quad \text{if } \alpha \text{ is irrational,}$$

$$k \geqq 0, \quad 1 \leqq l \leqq L, \quad 0 \leqq m \leqq \frac{k}{M} \quad \text{if } \alpha = \frac{M}{L} \text{ is rational.}$$

(M and L have no common divisor, and coefficients a_{klm} not needed are set at 0.) The terms in (4.1) are supposed to be arranged in appropriate order, which may deviate from the one shown explicitly. The expansion for g' is obtained by termwise differentiation and subsequent reordering [19]. For a simple deduction of the dominant term

in (4.1) see Warschawski [27], who, however, discusses the inverse map also covered by Lehman [19]. In case of a straight angle, i.e., $\alpha = 1$, (4.1) reduces to Lewy's expansion [20].

As in the usual deduction of Theodorsen's integral equation [4, p. 64], we note that there exists a continuous branch of $\log [g(w)/w]$ in $\bar{D}$ which takes the real value $\log g'(0)$ at 0. Consequently, the real continuous 2π-periodic functions X and Y defined by

$$X(t) + iY(t) := \log [e^{-it} g(e^{it})] \qquad (\forall t \in \mathbb{R}) \tag{4.2}$$

are conjugate periodic functions: $Y = KX$.

In particular, if we now assume that Γ is starlike with respect to 0 and given by its polar coordinate τ, $\rho(\tau)$, then $\theta(t) := Y(t) + t$ is the boundary correspondence function satisfying $g(e^{it}) = \rho(\theta(t))\, e^{i\theta(t)}$. Moreover, $\log \rho(\theta(t)) = X(t)$, and $Y = KX$ becomes Theodorsen's integral equation (1.7).

Whenever θ' exists, (4.2) yields

$$\theta'(t) = \operatorname{Im} \frac{ie^{it} g'(e^{it})}{g(e^{it})} = \operatorname{Re} \frac{e^{it} g'(e^{it})}{g(e^{it})}. \tag{4.3}$$

If we let $w = e^{it}$, $w_0 = e^{it_0}$ and insert (4.1) and the termwise differentiated series into (4.3), we get for $t \to t_0$ in view of $h = e^{it} - e^{it_0} = i(t - t_0) w_0 + O(|t - t_0|^2)$ and by choosing $\arg [i(t - t_0) w_0] = \arg (e^{it} - e^{it_0}) + O(|t - t_0|^2)$,

$$\theta'(t) \sim \operatorname{Re} \{b_{010} [(t - t_0) i w_0]^{\alpha - 1}\} = O(|t - t_0|^{\alpha - 1}), \tag{4.4}$$

where $b_{010} := \alpha a_{010} w_0 / g(w_0) \neq 0$, and similarly

$$\theta''(t) = O(|t - t_0|^{\alpha - 2}). \tag{4.5}$$

If $\alpha \neq 1$ and $\alpha \neq 2$, then $\operatorname{Re} \{\cdots\} \neq 0$, and the order stated is actually attained. In case $\alpha = 1$ we get

$$\theta'(t) \to \operatorname{Re} b_{010}, \qquad \theta''(t) = O(\log |t - t_0|), \tag{4.6}$$

while for $\alpha = 2$ we have $\operatorname{Re} \{b_{010} h^{\alpha - 1}\} = O(|t - t_0|^2)$, since Γ is starlike, so that even

$$\begin{aligned} \theta'(t) &= O(|t - t_0|^2 \log |t - t_0|), \\ \theta''(t) &= O(|t - t_0| \log |t - t_0|), \\ \theta'''(t) &= O(\log |t - t_0|). \end{aligned} \tag{4.7}$$

By making use of $K(H^m) \subset H^m$ [13, Lemma 9.1] and the fact that KY equals $-X$ up to a constant, we finally conclude:

$$\begin{aligned} &\theta,\ Y \text{ are absolutely continuous,} \\ &\theta',\ Y' \text{ are absolutely continuous iff } \alpha_j \geqq 1\ (\forall j), \\ &X,\ Y \in H^1 \text{ iff } \alpha_j > \tfrac{1}{2} (\forall j), \\ &X,\ Y \in H^2 \text{ iff } \alpha_j > \tfrac{3}{2} \text{ or } \alpha_j = 1\ (\forall j), \\ &X,\ Y \in H^3 \text{ iff } \alpha_j = 2\ (\forall j). \end{aligned} \tag{4.8}$$

As we have shown in [13], the function KS conjugate to the interpolating spline of degree $2m - 1$ is in a certain sense an optimal approximation for KX if only the values $X(t_k)$ and the information $X \in H^m$ are given. (4.8) allows us to choose the appropriate degree of the spline. In particular, we conclude that interpolating splines are not

appropriate if $\alpha_j \leqq \frac{1}{2}$ at some corner. However, smoothing splines and other smoothing approximants proved quite successful in our experiments, which are partly described in § 7. In case $\alpha_j \geqq 1$ $(\forall j)$ one might also try quadratic spline interpolation (with knots halfway between the data points).

5. Elimination of corners by preliminary maps. Under the initial assumptions of § 4, the mapping

$$\gamma_{\zeta_0,\alpha}: \zeta \in \bar{\Delta} \mapsto \hat{\zeta} := \zeta_0[1-(1-\zeta/\zeta_0)^{1/\alpha}] \tag{5.1}$$

offers itself as a means for eliminating the corner with interior angle $\alpha\pi (0<\alpha\leqq 2)$ at ζ_0. Of course, a continuous argument of $1-\zeta/\zeta_0$ has to be chosen in $\bar{\Delta}\backslash\{\zeta_0\}$ for the definition of $\gamma_{\zeta_0,\alpha}$, and we require that it be 0 at $\zeta = 0$. Then

$$\gamma_{\zeta_0,\alpha}(0) = 0, \qquad \gamma'_{\zeta_0,\alpha(0)} = \frac{1}{\alpha} > 0. \tag{5.2}$$

Moreover, $\gamma_{\zeta_0,\alpha}(\zeta_0) = \zeta_0$ and, if $\gamma_{\zeta_0,\alpha}(\bar{\Delta})$ is placed on a Riemann surface,

$$\gamma_{\zeta_0,1/\alpha} \circ \gamma_{\zeta_0,\alpha}(\zeta) = \zeta \qquad \forall \zeta \in \bar{\Delta}. \tag{5.3}$$

If the projection of $\gamma_{\zeta_0,\alpha}(\bar{\Delta})$ on $\mathbb{C}$ is not injective (as it may happen if $\alpha < 1$), a preliminary map $\gamma_{\zeta^*,1/\alpha}$ with a suitably chosen $\zeta^* \notin \bar{\Delta}$ usually enables us to avoid this situation. One could also replace $\gamma_{\zeta_0,\alpha}$ by a single but more complicated Kármán–Trefftz transformation,

$$\frac{\hat{\zeta}-\zeta_0}{\hat{\zeta}-\zeta^*} = \left(\frac{\zeta-\zeta_0}{\zeta-\zeta^*}\right)^{1/\alpha} \qquad \forall \zeta \in \bar{\Delta} \tag{5.4}$$

in this case, which occurs in practice less often than one would expect (cf. [36]). So, by a composition of conformal maps of the type (5.1), it is very often possible to eliminate all corners of Γ and to end up with a region Δ^* with boundary Γ^* in the plane. Yet, Γ^* is piecewise analytic only in a weaker sense, since its breakpoints are in general singular points of the analytic arcs joining there.

For particular applications the map (5.1), and many other preliminary conformal maps such as the Joukowski and the Kármán–Trefftz transformation, have been used for a long time (see [4, p. 257], [17], [26], [29]). For example, the success of Theodorsen's method in airfoil design would have been impossible without them [6]. But we would like to point out that one can nowadays develop a general and fairly reliable computer program for the successive elimination of all corners of many piecewise analytic curves. The main programming problem is choosing the correct argument of $1-\zeta/\zeta_0$. Another approach requiring the evaluation of indefinite integrals was described by Landweber and Miloh [18], but the composition of maps (5.1) is much simpler, its range of application is wider, and the inverse map is of the same type. It does not take care of axial symmetry, but the Kármán–Trefftz transformation could be applied instead of (5.1) to eliminate two symmetric corners at once. At the end, it is often profitable to apply additionally a Moebius transform T that keeps the origin fixed and maps the smallest circle containing Δ^* onto the unit disk. (A corresponding algorithm is described in [9].)

If the resulting region $T(\Delta^*)$ is not suitable for Theodorsen's method (e.g., because either it is not starlike or ε_ρ is too large) one could apply further auxiliary conformal maps such as those proposed by Koebe, Ringleb, Heinhold, and Albrecht for osculation methods (see [2], [4], [14], [26] and references given there). Grassmann [8] has reported on a recent computer implementation of such an osculation method. Our

examples given below (and many others) do not require such further preparatory maps, but it might be worthwhile to apply a few of them. The main handicap put by preliminary maps on the subsequent use of Theodorsen's method is that the boundary Γ^* [or $T(\Gamma^*)$] is no longer given in polar coordinates. So, one has to map a sufficient number of boundary points first, say the points $\zeta_{j,k}$, $k = 0, \cdots, k_j$, on the arc from $\zeta_j = \zeta_{j,0}$ to $\zeta_{j+1} = \zeta_{j+1,0} = \zeta_{j,k_j}$, $j = 1, \cdots, J$ (where $\zeta_{J+1} := \zeta_1$). We denote the image points by $\zeta^*_{k,j}$, and define $\arg \zeta^*$ continuously on Γ^* (assumed to be starlike with respect to 0) such that $\arg \zeta_1^* \leqq \arg \zeta^* \leqq \arg \zeta_1^* + 2\pi$. Then, we propose to interpolate the data $(\arg \zeta^*_{j,k}, \log |\zeta^*_{j,k}|)$, $k = 0, \cdots, j_k$, by a cubic spline s_j with double knots at the end points $\arg \zeta_j$ and $\arg \zeta_{j+1}$ (i.e. s_j interpolates there the derivative too). The global interpolation function

$$s(\tau) := s_j(\tau) \quad \text{if } \arg \zeta_j \leqq \tau \leqq \arg \zeta_{j+1} \quad (j = 1, \cdots, J) \tag{5.5}$$

replaces the function $\log \rho(\tau)$ in (1.1). Note that the $2N$ evaluations of s required afterwards in each iteration step for solving (1.1) are very cheap since the coefficients of s are computed only once.

One would like the abscissae $\arg \zeta^*_{k,j}$ roughly equidistant, but unfortunately the maps (5.1) cause strong distortions in arc length. When choosing $\zeta_{j,k}$, $k = 1, \cdots, k_j - 1$, it is at least possible to take the distortions at the two nearby breakpoints ζ_j^* and ζ_{j+1}^* approximately into account. In fact, $\zeta_{j,k}$ can be chosen in such a way that the points $\zeta^*_{j,k}$, $k = 0, \cdots, k_j$, would be equidistant if the arc from ζ_j to ζ_{j+1} were straight and these two corners were the only ones.

Of great importance to Theodorsen's method is the effect of the mapping (5.1) on the behavior of the boundary correspondence θ at some corner ζ_0. From (4.1) we get

$$\begin{aligned} \hat{g}(w_0 + h) &:= \zeta_0\{1 - [1 - g(w_0 + h)/\zeta_0]^{1/\alpha}\} \\ &\sim \zeta_0 + (-\zeta_0)^{1-1/\alpha_h}\Big[\sum_{k,l,m} a_{klm} h^{k+l\alpha-\alpha} (\log h)^m\Big]^{1/\alpha} \\ &= \zeta_0 + (-\zeta_0)^{1-1/\alpha} h\{a_{010}^{1/\alpha} + O(h^\alpha) + O(h \log h)\}, \end{aligned} \tag{5.6}$$

$$\hat{g}'(w_0 + h) = (-\zeta_0)^{1-1/\alpha} a_{010}^{1/\alpha} + O(h^\alpha) + O(h \log h), \tag{5.7}$$

$$\hat{g}''(w_0 + h) = O(h^{\alpha-1}) + O(\log h) \quad \text{as } h \to 0. \tag{5.8}$$

If α is irrational, $\log h$ can be replaced by 1 here.

If we eliminate all corners of Γ by preliminary maps of the type (5.1) and end up with a region Δ^* whose boundary Γ^* is starlike with respect to the origin, then—by the arguments used in § 4—the boundary correspondence function θ^* of a conformal map $g^* : D \to \Delta^*$ with $g^*(0) = 0$ and the related functions $Y^*(t) := \theta^*(t) - t$, $X^*(t) := \log \rho^*(\theta^*(t))$ satisfy in analogy to (4.8)

$$\begin{aligned} &d\theta^*/dt, dY^*/dt \quad \text{are absolutely continuous,} \\ &X^*, Y^* \in H^1, \\ &X^*, Y^* \in H^2 \text{ if } \alpha_j > \tfrac{1}{2} (\forall j). \end{aligned} \tag{5.9}$$

So, approximating X^* by a cubic spline is appropriate if $\alpha_j > \frac{1}{2}$ at every breakpoint of the piecewise analytic boundary Γ; otherwise, one may use a broken line interpolant, a slightly smoothed cubic spline approximant [13], a smoothed trigonometric interpolant, or, maybe, a quadratic spline interpolant.

Example 5.1. To the Swiss cross we first apply the map $\zeta \mapsto \zeta^4$ to account for the fourfold rotational symmetry. The resulting domain in Fig. 5.1(a) has three corners, which are removed by a composition of three maps of type (5.1) (see Fig. 5.1(b)–(d)). (The scale in these figures is not constant. The small squares mark removed corners.) An additional Moebius transform yields a boundary $T(\Gamma^*) \subset \bar{D}$ having three points in common with ∂D (cf. Fig. 5.1 (e)). Its point (marked by a square) nearest to 0 has modulus $\mu \doteq .903$, and ε is obviously small, so that a high accuracy approximation of $D \to T(\Delta^*)$ is easily computed by Theodorsen's method.

Example 5.2. The L-shape of Fig. 5.2(a) has six corners to eliminate (cf. Fig. 5.2(b)–(g)). After the Moebius transform, $\mu \doteq .593$ (see Fig. 5.2(h)). Twelve steps with Grassmann's osculation method program would lead to a boundary with $\mu \doteq .981$, but the inverse image of the unit circle under the corresponding composition of elementary transforms still deviates considerably from the given

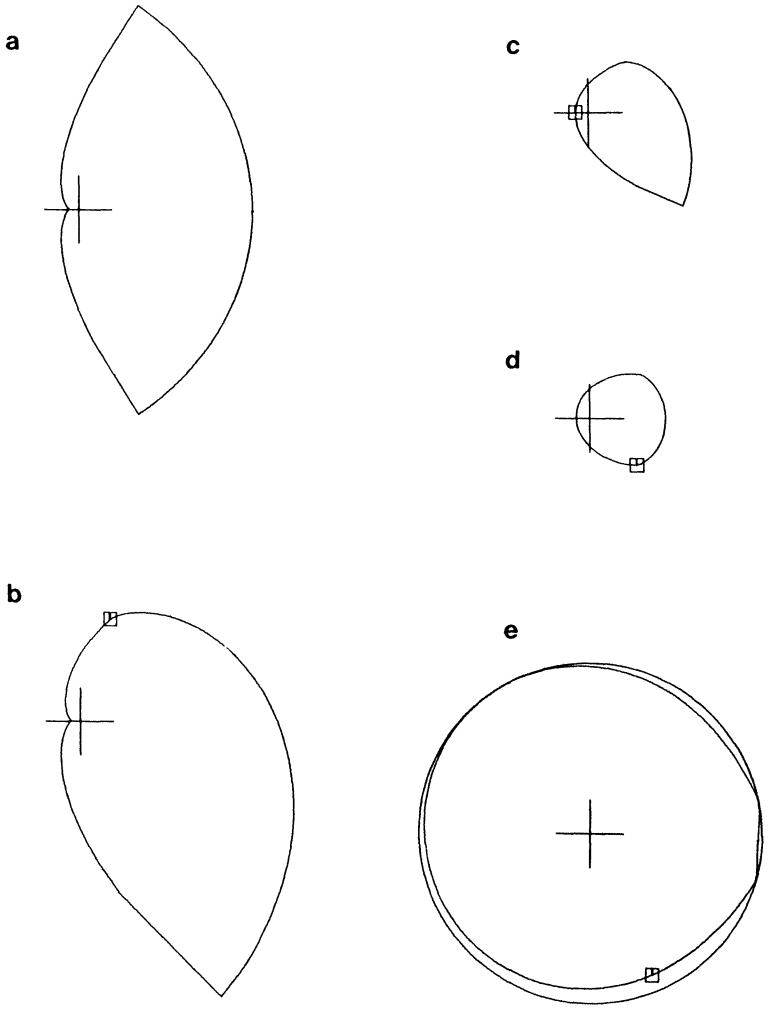

FIG. 5.1. *Elimination of the corners of a Swiss cross preliminarily mapped by* $\zeta \to \zeta^4$. *The three corners in* (a) *are removed one after another, cf.* (b)–(d), *then a Moebius transform is used to fit the region into the unit disk. The squares mark removed corners and, in* (e), *the point nearest to* 0, *respectively.*

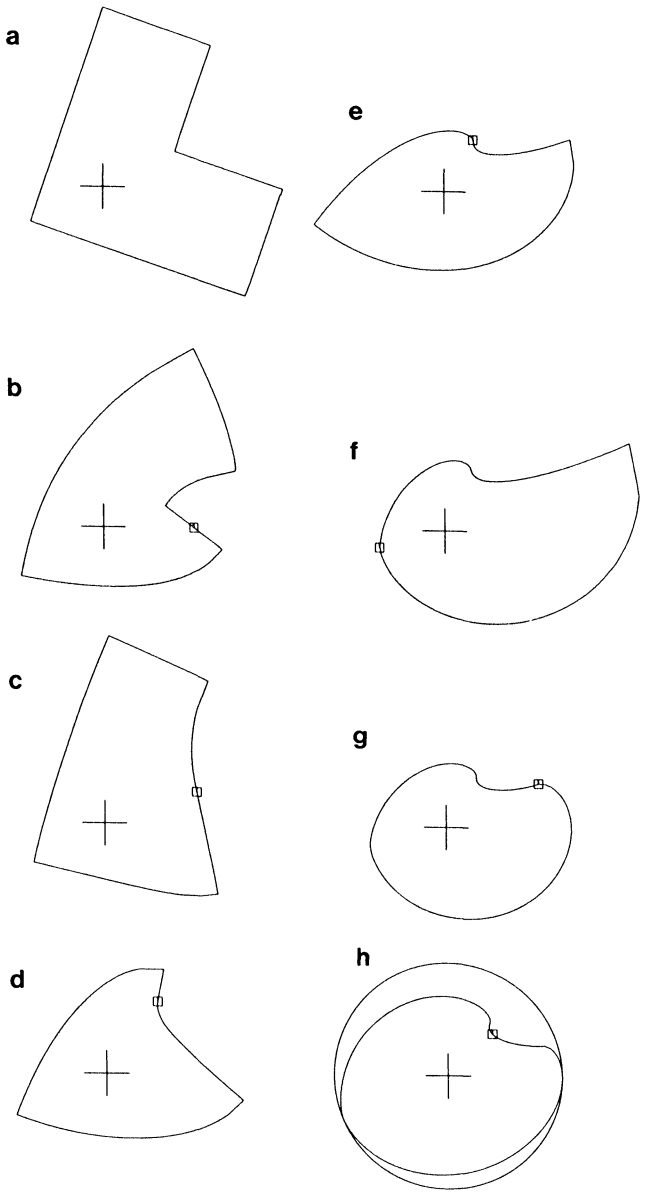

FIG. 5.2. *Elimination of the corners of an L-shape.*

L-shape. See Fig. 5.3, where the inverse image of 1,000 equidistant points on the unit circle is plotted. So, one still has to apply a more accurate method afterwards, such as e.g., Theodorsen's one, which can also be applied to the domain of Fig. 5.2(h) directly.

6. The evaluation of the mapping function and its derivative. Assume that $\mathbf{y}$ is a solution of the (original or modified) discrete Theodorsen equation (1.1). Then the components of $\boldsymbol{\theta} := \mathbf{t} + \mathbf{y}$ are approximate values of the boundary correspondence function θ. But how can we compute an approximate value of the conformal map $g : \bar{D} \to \bar{\Delta}$ at an arbitrary point $w \in \bar{D}$?

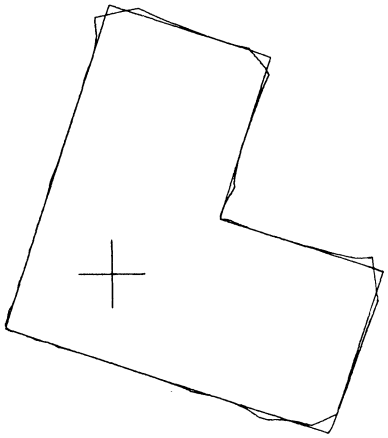

FIG. 5.3. *Inverse of the conformal mapping composed of six eliminations of corners, a Moebius transform, and twelve osculation maps.*

Again, denote by $P: \Pi_{2N}^{R} \to \mathscr{A}$ the operator upon which our discrete equation is based, and by $\boldsymbol{\tau} = (\tau_k) \in l_1$, its attenuation factors [13]. Let

$$\begin{aligned} \mathbf{x} &:= \log \rho(\mathbf{t}+\mathbf{y}), & \mathbf{c} &:= \mathscr{F}_{2N}\mathbf{x}, \\ X_N &:= P\mathbf{x}, & \mathbf{C} &:= \mathscr{F}X_N, \end{aligned} \tag{6.1}$$

so that $C_k = \tau_k c_k = \tau_{-k}\bar{c}_{-k} = \bar{C}_{-k} (\forall k \in \mathbb{Z})$ and

$$X_N(t) = \sum_{k=-\infty}^{\infty} C_k e^{ikt}, \qquad X_N(t) + i(KX_N)(t) = 2 \sum_{k=0}^{\infty}{}' C_k e^{ikt},$$

where the prime indicates that the term with index 0 has weight $\frac{1}{2}$. We conclude that

$$p_N(w) := 2 \sum_{k=0}^{\infty}{}' c_k \tau_k w^k \qquad (w \in \bar{D}) \tag{6.2}$$

is analytic in D, continuous in $\bar{D}$, and satisfies

$$\operatorname{Re} p_N(e^{it}) = X_N(t), \quad \operatorname{Im} p_N(e^{it}) = (KX_N)(t), \quad \operatorname{Im} p_N(0) = 0.$$

Due to the discrete Theodorsen equation (1.1),

$$(KX_N)(\mathbf{t}) = (KP\mathbf{x})(\mathbf{t}) = \mathbf{K}_{\Sigma}\mathbf{x} = \mathbf{y}. \tag{6.3}$$

If we define

$$g_N(w) := w \exp(p_N(w)), \tag{6.4}$$

we obtain

$$g_N(\exp(i\mathbf{t})) = \exp[(P\mathbf{x})(\mathbf{t}) + i\mathbf{y} + i\mathbf{t}]. \tag{6.5}$$

Consequently, if P is interpolatory, i.e., $(P\mathbf{x})(\mathbf{t}) = \mathbf{x}$,

$$g_N(\exp(it_k)) = \rho(t_k + y_k) \exp(it_k + iy_k) \in \Gamma, \qquad k = 0, \cdots, 2N-1. \tag{6.6}$$

So, $g_N : \bar{D} \to \mathbb{C}$ is a function that is analytic in D and has $2N$ image points $g_N(\exp(it_k))$ lying on Γ (if P is interpolatory). We may therefore hope that g_N is a reasonable approximation of g. However, in general we cannot guarantee this. For example, g_N may not be conformal due to loops of $g_N(\partial D)$ (see Example 7.4). Error bounds for

$g_N - g$ have only been given in case P stands for trigonometric interpolation and $\varepsilon < 1$ (see Gaier [4, pp. 92 ff.]).

For evaluating g_N at a single arbitrary point $w \in \bar{D}$ we might approximate p_N by a partial sum, which can be evaluated, e.g., by Horner's algorithm. However, we would like to point out a special formula in case w is of the form

$$w = re_{2\nu N}^{l} \qquad (0 < r \leqq 1,\ \nu \in \mathbb{Z},\ \nu > 0,\ l = 1, \cdots, 2\nu N) \tag{6.7}$$

where $e_{2\nu N} := \exp(i\pi/\nu N)$. Moreover, if r and ν are fixed, we can evaluate (or at least approximate) g_N simultaneously on the $2\nu N$ points of this type by using one FFT $\mathscr{F}_{2\nu N}^{-1}$. We think that in practice this property is an important advantage of Theodorsen's method. Also, an additional FFT yields the corresponding values of g_N', and we might proceed to compute higher derivatives.

Since $e_{2\nu N}^{2\nu N l} = 1$ $(\forall l \in \mathbb{Z})$, $\mathbf{c} \in \Pi_{2N} \subset \Pi_{2\nu N}$, and $\tau_{2jN} = 0$ for $j \neq 0$ [13, Eq. (2.5)], we obtain by inserting (6.7) into (6.2):

$$p_N(r e_{2\nu N}^{l}) = 2 {\sum_{k=0}^{2\nu N-1}}' c_k \chi_k^{(0)}(r) e_{2\nu N}^{kl}, \qquad l = 1, \cdots, 2\nu N, \tag{6.8}$$

where

$$\chi_k^{(0)}(r) := \sum_{j=0}^{\infty} \tau_{k+2\nu Nj} r^{k+2\nu Nj} \qquad (0 \leqq k < 2\nu N). \tag{6.9}$$

Similarly, if $(k\tau_k)_{k=-\infty}^{\infty} \in l_1$ or $r < 1$, differentiation of (6.2) yields

$$r e_{2\nu N}^{l} p_N'(r e_{2\nu N}^{l}) = 2 \sum_{k=1}^{2\nu N-1} c_k \chi_k^{(1)}(r) e_{2\nu N}^{kl}, \qquad l = 1, \cdots, 2\nu N, \tag{6.10}$$

where

$$\chi_k^{(1)}(r) := {\sum_{j=0}^{\infty}}' (k + 2\nu Nj) \tau_{k+2\nu Nj} r^{k+2\nu Nj} \qquad (1 \leqq k < 2\nu N). \tag{6.11}$$

The sums in (6.8) or (6.10) can be evaluated simultaneously at all $2\nu N$ points by applying $\mathscr{F}_{2\nu N}^{-1}$. Afterwards, (6.4) and

$$g_N'(w) = [1 + wp_N'(w)] \exp(p_N(w)) = [1 + wp_N'(w)] \frac{g_N(w)}{w} \tag{6.12}$$

yield the values of g_N and g_N', respectively, at these points. There remains the problem of summing up (6.9) and (6.11). We discuss two cases:

Example 6.1. Assume $\tau_k = 0$ for all $k > N$ as for *trigonometric interpolation* [13, Ex. 5.1], *Cesàro smoothing* or *Lanczos smoothing* [13, Ex. 6.1]. Then trivially

$$\chi_k^{(0)}(r) = \tau_k r^k, \qquad \chi_k^{(1)}(r) = k\tau_k r^k. \tag{6.13}$$

Example 6.2. If $r < 1$ and $2\nu N$ is sufficiently large, we may always approximate the series (6.9) and (6.11) by their first terms, i.e.,

$$\chi_k^{(0)}(r) \approx \tau_k r^k, \quad \chi_k^{(1)}(r) \approx k\tau_k r^k \quad \text{if } r < 1. \tag{6.14}$$

On the other hand, if $r = 1$ and P correspond to *interpolation by a spline function* S of degree $2m-1$ ($m \geqq 1$) [13, Ex. 5.2], we can sum up explicitly and obtain

$$\chi_k^{(0)}(1) = \begin{cases} \tau_0 & \text{if } k = 0, \\ \tau_k\left[1 + \psi_{2m-1}\left(\frac{k}{2\nu N}\right)\right] & \text{if } 0 < k < 2\nu N, \end{cases} \tag{6.15}$$

$$\chi_k^{(1)}(1) = k\tau_k\left[1 + \psi_{2m-2}\left(\frac{k}{2\nu N}\right)\right] \quad \text{if } 0 < k < 2\nu N \text{ and } m \geqq 2, \tag{6.16}$$

where the ψ_l are functions introduced in [13] and closely related to the polygamma functions $\psi^{(l)}$ [1, § 6.3]:

$$\psi_l(z) := \sum_{j=1}^{\infty}\left(\frac{z}{j+z}\right)^{l+1} = \frac{(-1)^{l+1}}{l!} z^{l+1}\psi^{(l)}(z) - 1$$

($z \in \mathbb{C}\backslash\{0, -1, -2, \cdots\}$, $l = 1, 2, \cdots$). Evaluating ψ_l is also discussed in [13, Ex. 5.2].

The formulas (6.14)–(6.16) also hold for smoothing by spline functions if we modify either c_k in (6.8) and (6.10) or τ_k in (6.14)–(6.16), cf. [13, § 6].

7. Numerical experiments on the accuracy of the approximate mapping function. As we have seen in the last section (cf. (6.6)), the $2N$ points $g_N(\exp(it_k))$ lie exactly on Γ if P is interpolatory and $\mathbf{y}$ is a solution of (1.1). So, for $t = t_k$

$$\delta_g(t) := \log|g_N(e^{it})| - \log\rho(\arg g_N(e^{it})) \tag{7.1}$$

should be 0, and thus, in addition to the residual defined by (2.5),

$$\delta_{g,0} := \max_k |\delta_g(t_k)| \tag{7.2}$$

is another measure for the accuracy of $\mathbf{y}$. For estimating the relative discretization error

$$\max_t |1 - g_N(e^{it})/g(e^{it})|, \tag{7.3}$$

we also compute

$$\delta_{g,1} := \max_k |\delta_g(t_k + t_1/2)|. \tag{7.4}$$

This estimate does not allow a direct comparison with the discretization error

$$\max_{\zeta\in\Gamma} |1 - |f_N(\zeta)|| \tag{7.5}$$

of approximations f_N to the inverse mapping $f = g^{[-1]}$, which is the aim of many other numerical mapping techniques [4], [5], [25]. But since

$$|\delta f| \approx |f'||\delta g| \approx \frac{|g|}{|g'|}|\delta \log g|,$$

we may consider

$$\delta_f(t) := \frac{|g_N(e^{it})|}{|g_N'(e^{it})|}\delta_g(t), \tag{7.6}$$

$$\delta_{f,0} := \max_k |\delta_f(t_k)|, \qquad \delta_{f,1} := \max_k |\delta_f(t_k + t_1/2)| \tag{7.7}$$

as estimates comparable to (7.5). They take into account that it is difficult to make $\delta_{g,1}$ small if $|wg_N'(w)|^{-1}$, the field strength of the potential field

$$\Psi_N(\zeta) := \log |g_N^{[-1]}(\zeta)| \quad \forall \zeta \in g_N(\bar{D}) \backslash \{0\} \tag{7.8}$$

becomes small on $g_N(\partial D)$.

Yet another crude accuracy test consists in plotting $g_N(\partial D)$ to compare it with Γ. In addition, one can easily plot equipotential lines $\Psi_N(\zeta) = \log r = \text{const}$ since many points on them can be computed with one FFT (cf. (6.8)). The corresponding field lines are crudely approximated by broken lines in the following plots, however.

Comparing $\delta_{g,0}$ or the residual with $\delta_{g,1}$ allows one to judge whether the discretization error is small enough, i.e., whether N is large enough. The quantities

$$v_{\min} := \min_t \left| \frac{g_N(e^{it})}{g_N'(e^{it})} \right|, \qquad v_{\max} := \max_t \left| \frac{g_N(e^{it})}{g_N'(e^{it})} \right| \tag{7.9}$$

(where usually only $t \in \{t_k, t_k + t_0/2, k = 0, \cdots, 2N-1\}$ in our tests) indicate whether the mapping problem is difficult to solve. Finally, $\delta_{f,0}$ and $\delta_{f,1}$ show whether $\boldsymbol{\theta} = \mathbf{y} + \mathbf{t}$ can serve as an accurate basis for determining the boundary correspondence function $t(\theta)$ of the inverse map by inverse interpolation. However, we must be aware that $v_{\min}$ and $v_{\max}$ may deviate essentially from the corresponding quantities for the exact mapping function g since g_N' may be an unsatisfactory approximation of g'. For the same reason, δf_0 and δf_1 may be poor estimates for (7.5).

Example 7.1. Results on the accuracy of the mapping function g_N corresponding to the SOR iterate $\mathbf{y}_{m(l)+1}$ for the inverse ellipse are given in Table 7.1. (For $\alpha = .1$ and $\alpha = .05$ the continuation method has been used.) If α is large (i.e., ε is small), $\delta_{g,0}$ and $\delta_{g,1}$ are of the same order, and they mainly depend on l, i.e., on the stopping criterion for the iteration (cf. (2.4)). If α is small, a reduction of the error $\delta_{g,1}$ requires a larger N. The quantities $v_{\min}$ and $v_{\max}$ have also been computed. At least five digits coincide with the correct values $v_{\min} = \alpha$, $v_{\max} = 1/\alpha$, except if $\alpha = .05$, where we obtain $v_{\min} = .050010$, $v_{\max} = 22.036$ (for $N = 128$), which indicates an error of at least 10% in g'. Plots of equipotential lines $\Psi_N(\zeta) = \log(k/8)$, $k = 1, \cdots, 8$, are shown in Fig. 7.1 for $\alpha = .2, .1$, and, partly, but five times magnified, for $\alpha = .05$.

TABLE 7.1
Accuracy of g_N^T for reflected ellipses (Ex. 7.1).

	$N = 32, l = 6$		$N = 128, l = 6$		$N = 128, l = 12$	
α	$\delta_{g,0}$	$\delta_{g,1}$	$\delta_{g,0}$	$\delta_{g,1}$	$\delta_{g,0}$	$\delta_{g,1}$
.8	$5.51_{10^{-11}}$	$4.42_{10^{-11}}$	$6.31_{10^{-11}}$	$5.25_{10^{-11}}$	$1.87_{10^{-14}}$	$1.60_{10^{-14}}$
.6	$1.90_{10^{-9}}$	$1.79_{10^{-9}}$	$2.43_{10^{-9}}$	$2.09_{10^{-9}}$	$3.91_{10^{-14}}$	$3.55_{10^{-14}}$
.4	$4.55_{10^{-8}}$	$1.65_{10^{-7}}$	$7.28_{10^{-8}}$	$7.07_{10^{-8}}$	$1.24_{10^{-13}}$	$1.39_{10^{-13}}$
.3	$2.87_{10^{-7}}$	$8.03_{10^{-6}}$	$3.12_{10^{-7}}$	$3.36_{10^{-7}}$	$1.99_{10^{-13}}$	$2.10_{10^{-13}}$
.2	$8.50_{10^{-7}}$	$5.43_{10^{-4}}$	$7.94_{10^{-7}}$	$9.18_{10^{-7}}$	$5.76_{10^{-13}}$	$1.14_{10^{-12}}$
.1	$1.52_{10^{-6}}$	$5.41_{10^{-2}}$	$1.36_{10^{-6}}$	$6.59_{10^{-7}}$	$3.54_{10^{-12}}$	$9.93_{10^{-7}}$
.05	$[3.59_{10^{-7}}$	$3.55_{10^{0}}]$	$2.78_{10^{-6}}$	$2.41_{10^{-3}}$	$1.65_{10^{-10}}$	$2.40_{10^{-3}}$

Examples 7.2 *and* 7.3 correspond to Examples 2.2 and 2.3, respectively. As shown in Table 7.2, $\delta_{g,1}$ is roughly of the same magnitude in the cases of trigonometric (T) and cubic spline interpolation (S3). The advantage of S3 becomes evident by

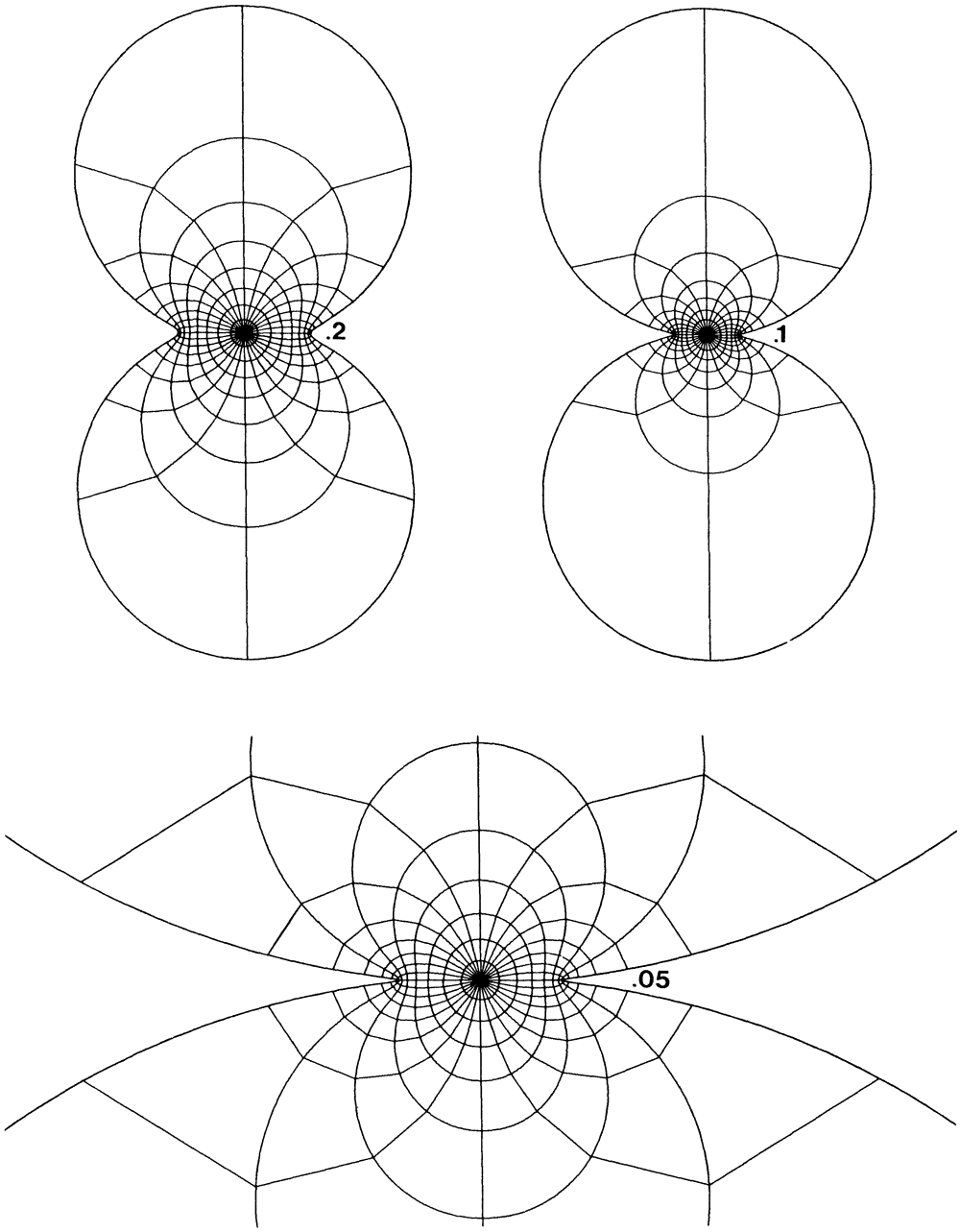

FIG. 7.1. *Conformal maps on reflected ellipses* ($\alpha = .2, .1,$ *and* $.05$).

inspection of g'_N. While $v^{\mathrm{T}}_{\min} = v^{\mathrm{S3}}_{\min}$, $v^{\mathrm{T}}_{\max} = v^{\mathrm{S3}}_{\max}$ for $\alpha = .4, .8$, we obtain for $\alpha = .2$, $N = 512$ in

$$\text{Ex. 2.1:} \quad v^{\mathrm{T}}_{\min} = .037, \quad v^{\mathrm{T}}_{\max} = 29.86,$$

$$\text{Ex. 2.2:} \quad v^{\mathrm{T}}_{\min} = .093, \quad v^{\mathrm{T}}_{\max} = 4.29.$$

TABLE 7.2
Accuracy of g_N^T and g_N^{S3} in case of a symmetric and in case of an asymmetric piecewise analytic boundary (Exs. 7.2 and 7.3).

		$N=128$		$N=512$					
Ex.	α	$\delta_{g,1}^T$	$\delta_{g,1}^{S3}$	$\delta_{g,1}^T$	$\delta_{g,1}^{S3}$	$\delta_{f,1}^T$	$\delta_{f,1}^{S3}$	v_{min}^{S3}	v_{max}^{S3}
7.2	.8	$2.52_{10^{-6}}$	$1.89_{10^{-6}}$	$3.09_{10^{-7}}$	$3.48_{10^{-7}}$	$2.40_{10^{-7}}$	$2.71_{10^{-7}}$	.774	1.25
	.4	$1.78_{10^{-3}}$	$1.47_{10^{-3}}$	$7.97_{10^{-5}}$	$1.02_{10^{-4}}$	$1.85_{10^{-5}}$	$2.34_{10^{-5}}$	.204	2.38
	.2	$\{1.02_{10^{-1}}\}$	$1.05_{10^{-1}}$	$9.78_{10^{-3}}$	$7.69_{10^{-3}}$	$2.27_{10^{-2}}$	$3.92_{10^{-4}}$	.049	5.02
7.3	.8	$6.37_{10^{-6}}$	$7.27_{10^{-6}}$	$4.30_{10^{-7}}$	$3.86_{10^{-7}}$	$3.85_{10^{-7}}$	$3.45_{10^{-7}}$	.847	1.27
	.4	$5.17_{10^{-4}}$	$6.43_{10^{-4}}$	$3.06_{10^{-5}}$	$3.15_{10^{-5}}$	$1.21_{10^{-5}}$	$1.24_{10^{-5}}$	.343	2.37
	.2	$2.18_{10^{-2}}$	$1.75_{10^{-2}}$	$3.35_{10^{-3}}$	$2.76_{10^{-3}}$	$4.31_{10^{-4}}$	$3.14_{10^{-4}}$	.096	4.04

The plots for these two examples are hardly distinguishable from the corresponding ones with S3 approximation shown in Fig. 7.2. However, the difference between T and S3 becomes visible if we reduce N to 128 as in Fig. 7.3. Here, g_N' is very inaccurate for both T and S3, of course.

Example 7.4. Results for the square and ten types of approximation (cf. Ex. 2.4) are compiled in Table 7.3. They have been computed by Euler iteration with $\mathbf{y}_0 = \mathbf{0}$, $l = 6$, $N = 1{,}024$ (actually, 256 variables are involved). The smallest error $\delta_{g,\max} := \max\{\delta_{g,0}, \delta_{g,1}\}$ is obtained for $S1/10^5$, the first degree smoothing spline with damping parameter $\tilde{\rho} = 10^5$. Unfortunately, in general g_N' has singularities on ∂D at the breakpoints e^{it_k} of the first degree spline. The best result among the

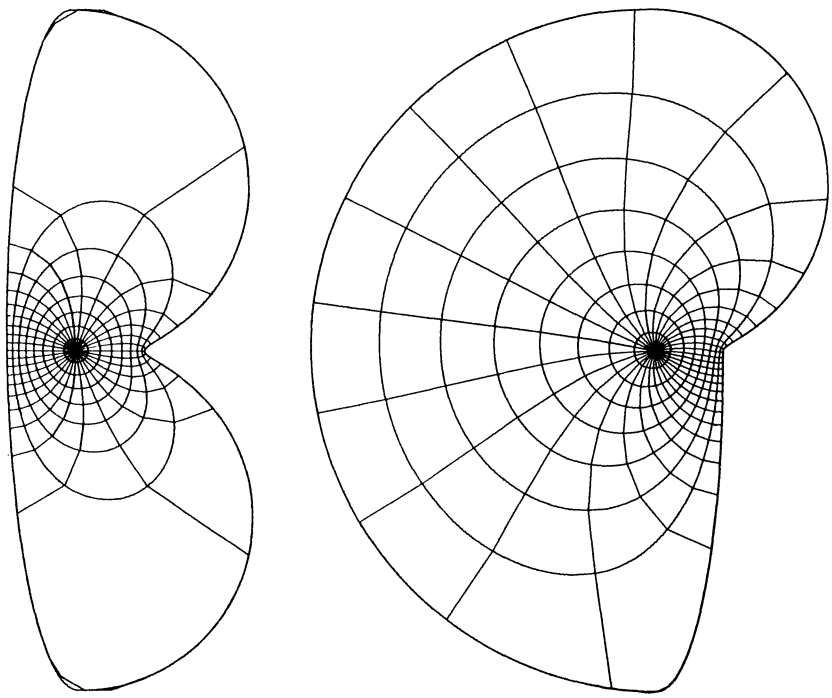

FIG. 7.2. *Examples* 7.2 *and* 7.3: *cubic spline interpolation with* $N = 512$.

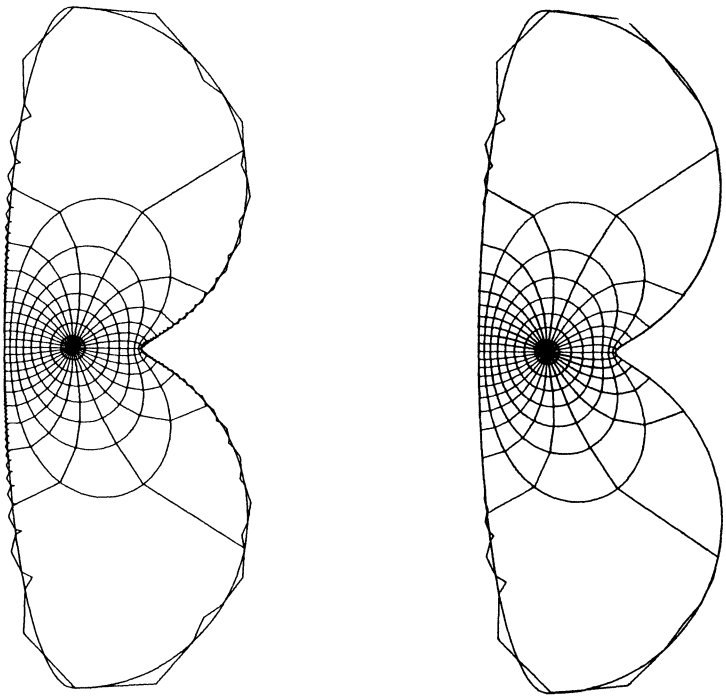

FIG. 7.3. *Example* 7.2: *trigonometric* (*left*) *and cubic spline* (*right*) *interpolation.*

TABLE 7.3
Accuracy of mapping functions based on various types of approximation (*Ex.* 7.4: *square*, $N = 1{,}024$).

	T	C	L	S3/10^8	S3/10^{10}	S3/10^{12}
$\delta_{g,0}$	$5.62_{10^{-8}}$	$1.92_{10^{-2}}$	$1.29_{10^{-2}}$	$1.64_{10^{-2}}$	$1.98_{10^{-3}}$	$6.81_{10^{-5}}$
$\delta_{g,1}$	$1.65_{10^{-2}}$	$5.81_{10^{-3}}$	$2.14_{10^{-3}}$	$5.65_{10^{-3}}$	$1.37_{10^{-2}}$	$1.56_{10^{-2}}$
$\delta_{f,0}$	$6.36_{10^{-8}}$	$2.03_{10^{-3}}$	$1.23_{10^{-3}}$	$1.63_{10^{-3}}$	$1.82_{10^{-4}}$	$6.17_{10^{-5}}$
$\delta_{f,1}$	$2.69_{10^{-3}}$	$6.32_{10^{-4}}$	$2.68_{10^{-4}}$	$7.03_{10^{-4}}$	$1.30_{10^{-3}}$	$1.48_{10^{-3}}$
$v_{\min}$	.0928	.1058	.0956	.0996	.0921	.0922
$v_{\max}$	1.3587	1.3374	1.3482	1.3281	1.3603	1.3604

	S1	S1/10^4	S1/10^5	S1/10^6
$\delta_{g,0}$	$3.00_{10^{-5}}$	$1.59_{10^{-2}}$	$3.70_{10^{-3}}$	$4.65_{10^{-4}}$
$\delta_{g,1}$	$9.33_{10^{-3}}$	$5.51_{10^{-3}}$	$6.18_{10^{-3}}$	$8.97_{10^{-3}}$

differentiable approximations considered is found for Lanczos smoothing. This has also been observed for some other regions with salient corners. Plots of the first quadrant are shown in Fig. 7.4. The one with trigonometric interpolation is magnified and based on 2,048 points of $g_N(\partial D)$ in this quadrant; $2N/4 = 512$ of these points should lie on Γ. This plot reveals that $g_N(\partial D)$ has loops. The other plots, for which only half as many points have been computed, exhibit that smoothing involves rounding off salient corners. The plot of S3/10^8, which is not shown, looks very similar to the one for L, and is therefore superior to the case S3/10^{10}, showing already a few ripples typical for S3.

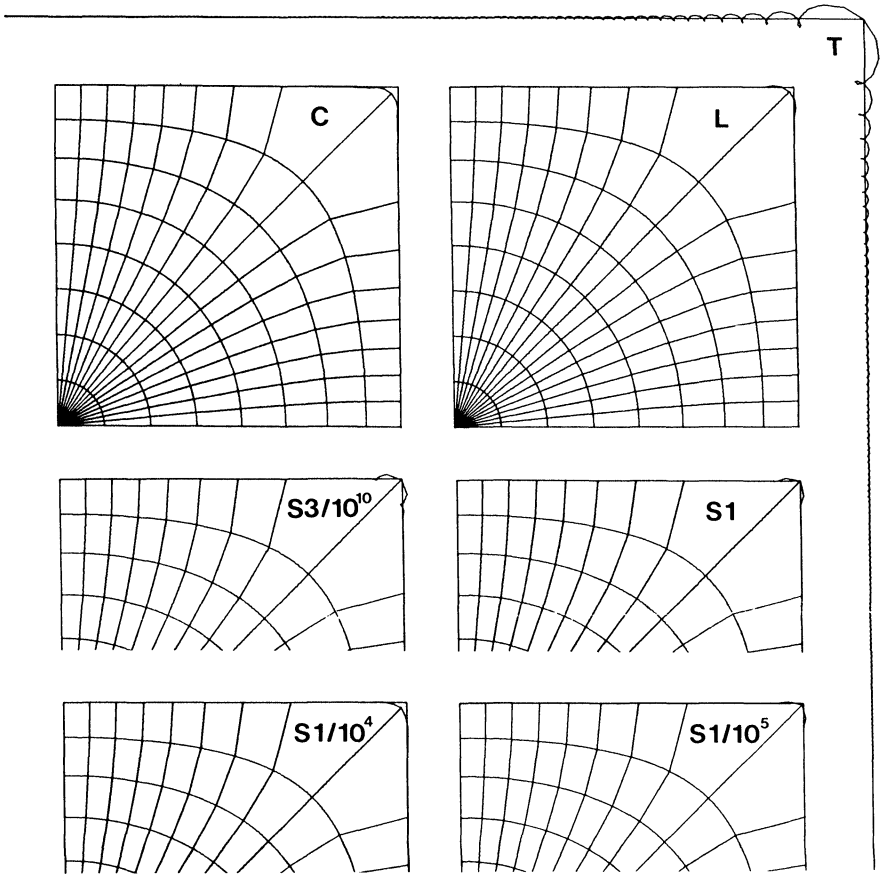

FIG. 7.4. *Conformal maps—based on various types of approximation—on a square.*

The behavior of $X(t) := \log \rho(\theta(t))$ in case of a piecewise analytic boundary (with $\varepsilon_\rho < \infty$, cf. § 4) suggests the conjecture that the loops in case of trigonometric interpolation can be avoided by choosing N large enough if $\alpha_j > \frac{1}{2}$ at all corners. (In fact, there are no loops if $\theta'_N(t) = Y'_N(t) + 1 > 0$ $(\forall t)$. Since $\theta' \in L_2[0, 2\pi]$ is piecewise continuous and positive except at corners with $\alpha_j > 1$, where $\theta'(t) = O(|t - t_j|^{\alpha_j - 1})$, one may expect that θ'_N is nonnegative and vanishes at most at these t_j if N is sufficiently large. As yet, a proof has not been given.)

In practice loops are a problem not only near corners with $\alpha_j \leqq \frac{1}{2}$. While theoretically no loops occur if Γ is analytic and N is sufficiently large, there are simple examples where it is in practice nearly impossible to avoid these loops:

Example 7.5. It is easy to map the disk fairly accurately onto an ellipse with semiaxes 1 and $\alpha = .4$. Yet, for $\alpha = .2$ we obtain the disappointing results listed in Table 7.4 and displayed in Fig. 7.5. Note that $\delta_{f,\max} := \max\{\delta_{f,0}, \delta_{f,1}\}$ is much smaller than $\delta_{g,\max} := \max\{\delta_{g,0}, \delta_{g,1}\}$ here. There is a marked similarity with the results for the square (and boundaries with acute corners). The best results are obtained by Lanczos smoothing and appropriately smoothed splines. Here, $S3/10^{10}$ is nearly as accurate as $S1/10^5$ (which is not differentiable). To obtain better results, one might try two preliminary Kármán–Trefftz transformations (cf. § 5 and [8]).

TABLE 7.4
Accuracy of mapping functions based on various types of approximation (Ex. 7.5: ellipse with $\alpha = .2$).

N		T	C	L	S3	S3/10^6	S3/10^8	S3/10^{10}
512	$\delta_{g,max}$	{.4348}	.2182	.1836	{.4165}	.3400	.2187	{.3487}
1024	$\delta_{g,max}$	{.3235}	.1673	.1385	{.3086}	.3400	.2240	.1170
	$\delta_{f,max}$	.0571	.0677	.0303	.0187	.0189	.0054	.0019
	v_{min}	.0167	.0179	.0167	.0165	.0555	.0242	.0163
	v_{max}	1.8248	1.7476	1.8066	1.8350	1.5497	1.5552	1.8402

N		S1	S1/10^4	S1/10^5	S1/10^6
512	$\delta_{g,max}$	{.2705}	.1912	{.1824}	{.2600}
1024	$\delta_{g,max}$	{.1876}	.2159	.0975	{.1563}

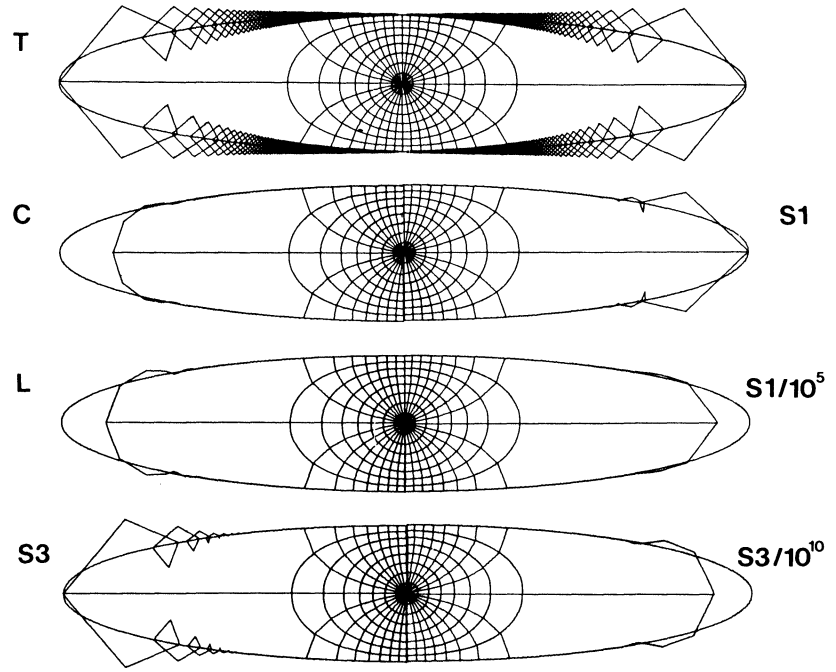

FIG. 7.5. *Seven types of approximate conformal maps on an ellipse.*

Example 7.6. Results for the Swiss cross, which is an example with a reentrant corner, are compiled in Table 7.5 ($N = 2{,}048$). The two examples in the top part of Fig. 7.6 demonstrate that $N = 512$ (i.e., 128 variables) is enough for a rough but reasonable approximation. All six other solutions in Fig. 7.6 are done with $N = 2{,}048$.

Example 7.7. In Fig. 7.7 we display the Lanczos type solution with $N = 512$ for an asymmetric L-shape. It confirms that the method also works for asymmetric regions.

So far, we have done no tests on the accuracy of the conformal mapping defined by composition of g_N, optional inverse osculation maps, and the maps inverse to those

TABLE 7.5

Accuracy of mapping functions based on various types of approximation (Ex. 7.6: Swiss cross, $N = 2{,}048$).

	T	C	L	S3/10^8	S3/10^{10}	S3/10^{12}
$\delta_{g,\max}$	$7.66_{10^{-3}}$	$2.30_{10^{-2}}$	$2.02_{10^{-2}}$	$2.80_{10^{-2}}$	$2.10_{10^{-2}}$	$6.79_{10^{-3}}$
$\delta_{f,\max}$	$2.86_{10^{-3}}$	$1.27_{10^{-2}}$	$9.28_{10^{-4}}$	$1.69_{10^{-3}}$	$9.40_{10^{-4}}$	$1.48_{10^{-3}}$
$v_{\min}$	.0442	.0464	.0459	.0602	.0448	.0443
$v_{\max}$	54.43	27.08	39.53	26.10	47.47	64.58

	S1	S1/10^5	S1/10^6	S1/10^7	S1/10^8
$\delta_{g,\max}$	$1.59_{10^{-2}}$	$2.05_{10^{-2}}$	$1.88_{10^{-2}}$	$1.62_{10^{-2}}$	$1.60_{10^{-2}}$

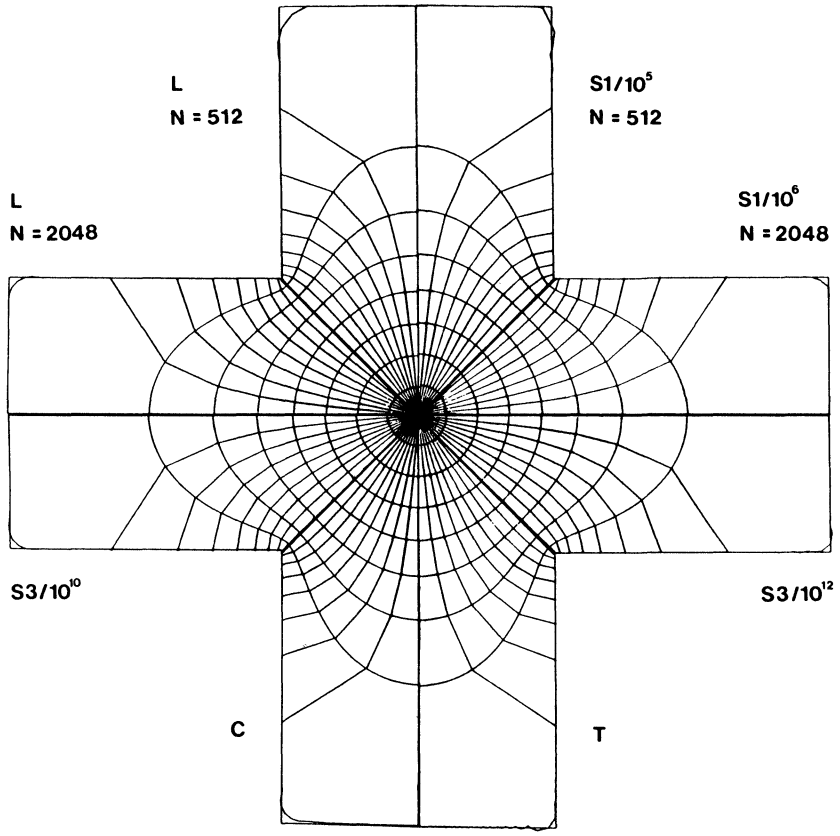

FIG. 7.6. *Eight types of approximate conformal maps on a Swiss cross. (Inaccuracies on the symmetry axes are due to inaccurate plotting and gluing.)*

used for corner elimination (cf. § 5). However, the following should be kept in mind: If $\delta_g(t_0)$ is the error of g_N at a point t_0, where a corner with angle $\alpha\pi$ has been eliminated, then the inverse transformation, which contains a map of type $\gamma_{\zeta_0,1/\alpha}$, yields an error proportional to $[\delta_g(t_0)]^\alpha$. So, if α is small, much of the accuracy of Theodorsen's method (or any other one) gets lost.

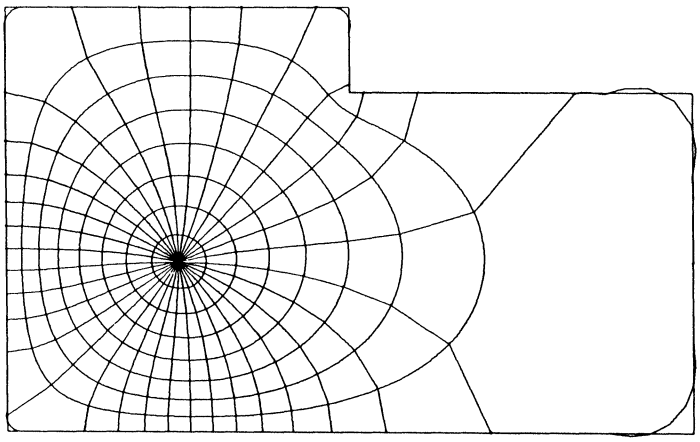

FIG 7.7. *Conformal map (with Lanczos smoothing) on an L-shape.*

8. Conclusions. The nonlinear SOR iteration and the nonlinear second order Euler iteration proposed in [12] are efficient means for solving the classical or the modified discrete Theodorsen equation, respectively, for most regions that are starlike with respect to the origin. If $\varepsilon_\rho > 1$, one may have to apply the continuation method of § 3 as an outer iteration. But then, in all of our tests convergence was achieved if N and the parameters I_0 and l_0 of the continuation method were large enough.

However, the classical discretization based on trigonometric interpolation may yield approximate mapping functions g_N which are useless since they are not one-to-one. Not only does this happen for boundaries with acute corners, but in practice even for certain simple analytic boundaries where the mapping problem is ill-conditioned, such as, e.g., flat ellipses. Discretizations based on other types of approximation involving some smoothing yield much better results in these cases. Smoothing has the (in practice often negligible) effect of rounding off salient corners and other salient parts of the region, where the Green's function nearly vanishes. In particular, Cesaro and Lanczos smoothing proved very useful. (For similar smoothing techniques not tested here, see [32], [37], [38].) Smoothing splines, which are more difficult to implement but nearly as efficient in execution, may yield even better results if the smoothing parameter is chosen appropriately (which was done by trial and error in our tests). First degree splines are not suitable if g'_N is requested too.

If we cannot allow salient corners to be rounded off, we can usually eliminate these corners by preliminary conformal maps, which have also been implemented in a general program. Additional preliminary osculation maps could be used to deal with regions that are not starlike or that present other difficulties. More tests in this direction are certainly worthwhile.

Acknowledgment. I am indebted to Prof. P. Henrici for his continuous interest in and support for this project. I have also benefited from valuable discussions with the late Prof. E. Grassmann, whose work in numerical conformal mapping was abruptly terminated by his tragic premature death.

Furthermore, I am very grateful to Miss B. Knecht, who typed this and several related manuscripts with utmost care, and to my wife Ursula for the patience and understanding which allowed me to complete this work. Finally, L. N. Trefethen and an unknown referee were kind enough to suggest a number of linguistic improvements.

REFERENCES

[1] M. ABRAMOWITZ AND I. A. STEGUN, *Handbook of Mathematical Functions*, National Bureau of Standards, Washington, DC, 1964.

[2] R. ALBRECHT, *Zum Schmiegungsverfahren der konformen Abbildung*, Z. Angew. Math. Mech., 32 (1952), pp. 316–318.

[3] J. W. COOLEY, P. A. W. LEWIS AND P. D. WELCH, *The finite Fourier transform*, IEEE Trans. Audio Electroacoust. AU-17 (1969), pp. 77–85.

[4] D. GAIER, *Konstruktive Methoden der konformen Abbildung*, Springer, Berlin/Göttingen/Heidelberg, 1964.

[5] ———, *Integralgleichungen erster Art und konforme Abbildung*, Math. Z., 147 (1976), pp. 113–129.

[6] I. E. GARRICK, *Conformal mapping in aerodynamics, with emphasis on the method of successive conjugates*, National Bureau of Standards Appl. Math. Ser., 18 (1952), pp. 137–147.

[7] W. GAUTSCHI, *Attenuation factors in practical Fourier analysis*, Numer. Math., 18 (1972), pp. 373–400.

[8] E. GRASSMANN, *Numerical experiments with a method of successive approximation for conformal mapping*, Z. Angew. Math. Phys., 30 (1979), pp. 873–884.

[9] E. GRASSMANN AND J. G. ROKNE, *The range of values of a circular complex polynomial over a circular complex interval*, Computing, 23 (1979), pp. 139–169.

[10] M. H. GUTKNECHT, *Existence of a solution to the discrete Theodorsen equation for conformal mappings*, Math. Comp., 31 (1977), pp. 478–480.

[11] ———, *Fast algorithms for the conjugate periodic function*, Computing, 22 (1979), pp. 79–91.

[12] ———, *Solving Theodorsen's integral equation for conformal maps with the fast Fourier transform and various nonlinear iterative methods*, Numer. Math., 36 (1981), pp. 405–429.

[13] ———, *Solving Theodorsen's integral equation for conformal maps with the fast Fourier transform, Part III: The evaluation of the conjugate function of a periodic spline on a uniform mesh*, Report 79-05, Seminar f. Angew. Math., Eidgen. Tech. Hochschule, Zürich, Oct. 1979.

[14] J. HEINHOLD AND R. ALBRECHT, *Zur Praxis der konformen Abbildung*, Rend. Circ. Mat. Palermo Ser. 2, 3 (1954), pp. 130–148.

[15] P. HENRICI, *Fast Fourier methods in computational complex analysis*, SIAM Rev., 21 (1979), pp. 481–527.

[16] O. HÜBNER, *Zur Numerik der Theodorsenschen Integralgleichung in der konformen Abbildung*, Mitt. Math. Sem. Giessen, 140 (1979), pp. 1–32.

[17] H. KOBER, *Dictionary of Conformal Representation*, Dover, New York, 1952.

[18] L. LANDWEBER AND T. MILOH, *Elimination of corners in the mapping of a closed curve*, J. Engrg. Math., 6 (1972), pp. 369–375.

[19] R. S. LEHMAN, *Development of the mapping function at an analytic corner*, Pacific J. Math., 7 (1957), pp. 1437–1449.

[20] H. LEWY, *Developments at the confluence of analytic boundary conditions*, Univ. of California Publ. in Math., 1 (1950), pp. 247–280.

[21] C. LUNDWALL-SKAAR, *Konforme Abbildung mit Fast Fourier Transformationen*, Diplomarbeit, Eidgen. Tech. Hochschule, Zürich, 1975.

[22] W. NIETHAMMER, *Iterationsverfahren bei der konformen Abbildung*, Computing, 1 (1966), pp. 146–153.

[23] J. M. ORTEGA AND W. C. RHEINBOLDT, *Iterative Solution of Nonlinear Equations in Several Variables*, Academic Press, New York, 1970.

[24] R. C. SINGLETON, *An algorithm for computing the mixed radix fast Fourier transform*, IEEE Trans. Audio Electroacoust., AU-17 (1969), pp. 93–103.

[25] G. T. SYMM, *An integral equation method for conformal mapping*, Numer. Math., 9 (1966), pp. 250–258.

[26] W. VON KOPPENFELS AND F. STALLMANN, *Praxis der konformen Abbildung*, Springer, Berlin/Göttingen/Heidelberg, 1959.

[27] S. E. WARSCHAWSKI, *On a theorem of L. Lichtenstein*, Pacific J. Math., 5 (1955), pp. 835–840.

[28] R. WEGMANN, *Ein Iterationsverfahren zur konformen Abbildung*, Numer. Math., 30 (1978), pp. 453–466.

[29] J. R. WHITEMAN AND S. SCHEFFLER, *Conformal transformation techniques for the numerical solution of Poisson problems*, Report BICOM 78-3, Institute of Computational Mathematics, Brunel University, Uxbridge, England, June 1978.

[30] F. BAUER, P. GARABEDIAN, D. KORN AND A. JAMESON, *Supercritical Wing Sections* II, Springer, Berlin/Heidelberg/New York, 1975.

[31] S. CHAKRAVARTHY AND D. ANDERSON, *Numerical conformal mapping*, Math. Comp., 33 (1979), pp. 953–969.

[32] A. K. CHAN AND C. K. CHUI, *Nonrecursive digital filter designs by means of Korovkin kernels*, IEEE Trans. Acoust. Speech Signal Process., ASSP-27 (1979), pp. 218–222.
[33] B. FORNBERG, *A numerical method for conformal mappings*, this Journal, 1 (1980), pp. 386–400.
[34] M. H. GUTKNECHT, *Two applications of periodic splines*, in Approximation Theory III, E. W. Cheney, ed., Academic Press, New York, 1980.
[35] R. M. JAMES, *A new look at two-dimensional incompressible airfoil theory*, Report MDC-J0918/01, Douglas Aircraft Company, 1971.
[36] G. MORETTI, *Conformal mappings for computations of steady, three-dimensional, supersonic flows*, in Numerical/Laboratory Computer Methods in Fluid Mechanics, American Society of Mechanical Engineers, New York, 1976.
[37] A. H. NUTTAL, *Some windows with very good sidelobe behavior*, IEEE Trans. Acoust. Speech Signal Process., ASSP-29 (1981), pp. 84–91.
[38] C. ROSSI, *Window functions for nonrecursive digital filters*, Electron. Lett., 3 (1967), pp. 559–561.
[39] L. C. WOODS, *The Theory of Supersonic Plane Flow*, Cambridge Univ. Press, Cambridge, 1961.